SIMULATION OF A SILICON NANOWIRE FET BIOSENSOR FOR DETECTING BIOTIN/STREPTAVIDIN BINDING

by

Yucai Wang

B.S. in Microelectronics, Fudan University, China, 2004

M.S. in Microelectronics, Shanghai Institute of Microsystem and Information Technology, Chinese Academy of Sciences, China, 2007

Submitted to the Graduate Faculty of

The Swanson School of Engineering in partial fulfillment

of the requirements for the degree of

Master of Science

University of Pittsburgh

2010

UNIVERSITY OF PITTSBURGH

SWANSON SCHOOL OF ENGINEERING

This thesis was presented

by

Yucai Wang

It was defended on

July 23, 2010

and approved by

Dr. Guangyong Li, Assistant Professor, Departmental of Electrical and Computer Engineering

Dr. Mahmoud El Nokali, Associate Professor, Departmental of Electrical and Computer Engineering

Dr. Kevin Chen, Associate Professor, Departmental of Electrical and Computer Engineering

Thesis Advisor: Dr. Guangyong Li, Departmental of Electrical and Computer Engineering

SIMULATION OF A SILICON NANOWIRE FET BIOSENSOR FOR DETECTING

BIOTIN/STREPTAVIDIN BINDING

Yucai Wang, M.S.

University of Pittsburgh, 2010

Silicon nanowire field-effect transistor (SiNW FET) biosensors have recently been demonstrated experimentally for direct, label free, high sensitive, high selective and real time detection of DNA and proteins at very low concentration.

Among these experiments, the detection of biotin/streptavidin binding is of special interest since the biotin/streptavidin system exhibits one of the strongest noncovalent biological interactions known in nature. Thus, biotin/streptavidin system is widely demonstrated as a model system to study biorecognition between proteins and other biomolecules.

Despite these promising experimental results and their enormous potential, it is somewhat surprising that the fundamental mechanism of electrical sensing of biomolecules and the design principles of SiNW FET biosensor remain poorly understood.

In this work, a comprehensive modeling theory and simulation approach is presented to account for the underlying detection mechanism of biotin/Streptavidin binding using SiNW FET biosensor. The influence of parameters like the dimension of the SiNW, the doping of the SiNW, and surrounding environment (the ions concentration in the solvent) are investigated for the performance optimization of the SiNW FET biosensor. The preliminary simulation results indicate that the optimal sensor performance can be ensured by careful optimization of its parameters and it is feasible to detect binding of single streptavidin molecule when optimal parameters are chosen.

TABLE OF CONTENTS

LIST OF TABLES

LIST OF FIGURES

PREFACE

I first thank my advisor, Dr. Guangyong Li, for his relentless support, instruction and advice. Without his astute guidance, I could never have done this work. Even more importantly, his enthusiasm in innovations, attitude towards research and optimism deeply impressed and encouraged me. I am grateful to Dr. Li on a professional and personal level.

I also thank Professor El Nokali and Professor Chen for joining my committee and giving me precious advice on my thesis. I further thank my fellow researcher, Liming Liu, for his continuous aid to my research and everyday life.

I would like to thank my local friends, Mr. Robert W. Thomson's family for making my stay in Pittsburgh a pleasant experience.

Finally, special thanks to my family for their unlimited love, encouragement and support.

1.0   INTRODUCTION

1.1   MOTIVATION

In recent years, electronic detection of biomolecules in the solvent is one of the widely studied topics in nanotechnology. Systems based on nanoscale devices can provide fast, low-cost, and high throughput analysis of biological processes and are gaining importance due to their large potential in commercial applications, ranging from detection of protein, virus and DNA to the discovery of new drug delivery systems [1].

Since the early 1970s, the basic idea of ion-selective field-effect transistor (ISFET) has been realized based on metal oxide silicon field-effect transistor (MOSFET) [2]. In an ISFET the gate structure of a MOSFET is replaced by a biomaterial layer (ion-selective layer), electrolyte and a reference electrode. The ISFET can measure the concentration of certain ion species in the electrolyte, such as protein, enzyme and DNA [3]. It was regarded as a low-cost alternative to traditional chemical sensors with potential for on-chip integration [4]. However, several disadvantages, such as lack of good solid state electrodes, parasitic sensitivity to temperature and light, time dependent instability of sensor parameters, have restrained the development of ISFET as a popular biosensor technology [5].

The significant technological advances in silicon very-large-scale-integration have made fabrication of SiNW FET biosensors possible. These biosensors consist of a SiNW core, a

surrounding silicon oxide layer, a layer of biomaterial, and surface receptor biomolecules. The specific binding of a few charged target biomolecules onto the receptor molecules can modulate the carriers' distribution inside the SiNW. Because of the small size and large surface-to-volume ratio of the SiNW, the detecting sensitivity is increased as compared with traditional ISFET biosensors [1].

SiNW FET biosensors have already demonstrated ultrasensitive detection of DNA, proteins, pH levels, etc. Thus, it is possible that arrays of SiNW FET biosensors will be able to detect a huge class of biomolecules. The major advantage of SiNW FET biosensors is the label free operation, as opposed to the expensive and time-consuming preprocessing and postprocessing for sample preparation and data analysis in chemical detection. Other advantages include the high sensitivity and the real time and continuous operation.

Among the demonstrated experiments, the detection of biotin/streptavidin (or avidin) binding is of special interest and is widely demonstrated as a model system to study biorecognition between proteins and other biomolecules [6]. The biotin/streptavidin system, with a binding affinity of 10^{15} M^{-1} for free complexes, exhibits one of the strongest noncovalent biological interactions known in nature [7]. This binding couple remains highly stable under various harsh conditions, including extreme pH, salt concentration, and temperature. Biomolecules such as proteins and DNA can be easily biotinylated and bound to streptavidin coated surfaces.

Despite these promising experimental results of SiNW FET biosensors and their enormous potential in commercial applications, it is somewhat surprising that the fundamental mechanism of electrical sensing of biomolecules and the design principles of SiNW FET biosensor remain poorly understood. Many parameters affect the performance of SiNW FET biosensor, such as the

dimension of the SiNW, the doping density of the SiNW, the surrounding environment (the ions concentration in the solvent). These parameters need to be investigated for the systematic optimization of biosensor design [1].

In this thesis, a comprehensive modeling theory and simulation approach is proposed to account for the underlying electrical detection mechanism of biotin/Streptavidin binding using SiNW FET biosensor. The theory is based on drift-diffusion equation of the SiNW and Poisson Boltzmann equation for the biomolecules and solvent system [8]. The Poisson Boltzmann equation is derived from the classical Poisson equation using the Boltzmann distribution to model the charge distribution in the ionic solvent. The analytical and numerical solutions to the Poisson Boltzmann equation are discussed. The detailed structures, modeling procedure and simulation methods of the SiNW FET biosensor are presented. The simulation results are analyzed and the influence of parameters like the dimension of the SiNW, the doping of the SiNW, and surrounding environment (the ions concentration in the solvent) are investigated for the performance optimization of the SiNW FET biosensor. Also, the detection limit of biotin/Streptavidin binding using the SiNW FET biosensor, i.e., the detection of single streptavidin molecule binding is investigated and validated.

1.2   THESIS ORGANIZATION

Chapter 2 gives a brief background of this research. This chapter is divided into two parts. The first part gives background of ISFET, nanowire FET and silicon nanowire FET biosensor. The basic operation principle of ISFET and SiNW FET biosensor are included. The properties and advantages of SiNW are presented. Two popular SiNW fabrication techniques are

introduced and their advantages and disadvantages are discussed. The concept of using SiNW as biosensor is presented and the advantages of SiNW FET sensor are introduced. The second part focuses on the derivation of Poisson-Boltzmann equation. Poisson-Boltzmann equation is derived from the classical Poisson equation using the Boltzmann distribution to model the charge distribution in the ionic solution. Analytical solutions of the Poisson-Boltzmann equation for two special cases are discussed. Also, several popular numerical methods for solving the Poisson-Boltzmann equation are introduced.

Chapter 3 introduces the detailed structure of SiNW FET biosensor. The comprehensive modeling theory and simulation approach are presented to account for the underlying detection mechanism of biotin/Streptavidin binding using SiNW FET biosensor. The simulation softwares and detailed simulation procedures are introduces.

Chapter 4 deals with the simulation results with detailed analysis. The influence of parameters like the dimension of the SiNW, the doping of the SiNW, and surrounding environment (the ions concentration in the solvent) are investigated for the performance optimization of the SiNW FET biosensor. The detection limit of biotin/Streptavidin binding using the SiNW FET biosensor is also investigated and validated.

Chapter 5 draws the conclusions and summarizes the accomplishments of this work. The potential application of our research and possible future work are included.

2.0   BACKGROUND

2.1   INTRODUCTION TO FET BIOSENSORS

2.1.1   ISFET

Since the early 1970s, the basic idea of ion-selective field-effect transistor (ISFET) has been realized based on MOSFET. The ISFET can measure ion concentrations (such as pH) in solution; the current through the transistor will change accordingly when the ion concentration changes. A basic scheme of ISFET is shown in Figure 2.1. The simple modification from MOSFET to ISFET is to remove the gate surface metallization of a MOSFET and connect the gate oxide to a reference electrode (the gate electrode) via an aqueous solvent.

The basic operation principle of ISFET is similar to MOSFET. The drain current of the MOSFET and the ISFET in the non-saturated mode can be expressed using a general equation:

$$I_d = C_{ox}\mu\frac{W}{L}[(V_{gs} - V_t)V_{ds} - \frac{1}{2}V_{ds}^2] \quad (2.1)$$

where C_{ox} is gate insulator capacitance per unit area, W and L are the width and the length of the channel, respectively, μ is the electron mobility in the channel, V_{gs} is the gate-source voltage bias, V_{ds} is the drain-source voltage bias and V_t is the threshold voltage value.
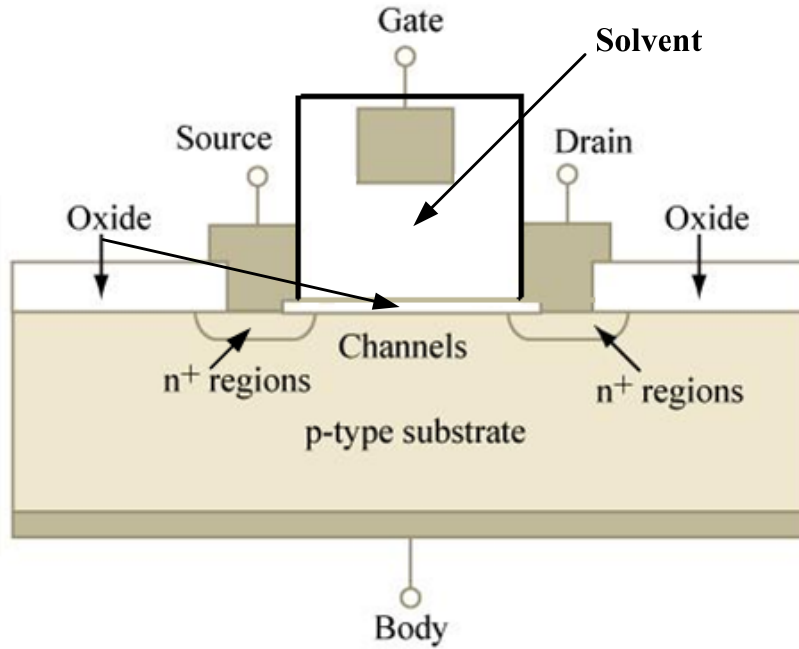
Figure 2.1 Scheme of an ISFET

The geometric sensitivity parameter $\beta = C_{ox} \mu W/L$ is constant; the drain-source voltage bias V_{ds} is set constant via external circuit.

The threshold voltage V_t is given by:

$$V_t = V_{FB} - \frac{Q_B}{C_{ox}} + 2\phi_F \qquad (2.2)$$

where V_{FB} is the flat band voltage, Q_B is the depletion charge in the silicon and Φ_F is the Fermi potential.

For the MOSFET, the flat band voltage can be expressed as [9]:

$$V_{FB} = \frac{\Phi_M - \Phi_{Si}}{q} - \frac{Q_{ss} + Q_{ox}}{C_{ox}} \qquad (2.3)$$

where Φ_M is the work function of the gate metal, Φ_{Si} is the silicon work function, Q_{ss} is the surface state density at the silicon surface and Q_{ox} is the fixed oxide charge.

6

From equation (2.2) and (2.3) it can be seen that the threshold voltage of MOSFET is determined by the material properties and the fabrication process. Thus, for a given MOSFET the threshold voltage is constant. From equation (2.1) now we can see that for a MOSFET the drain current I_d is a unique function of the gate-source voltage bias V_{gs}.

In the case of ISFET the difference in gate structure results in a different expression of flat band voltage. Two factors contribute to modification of the flat band voltage expression: the constant potential of the reference electrode, E_{ref}, and the interfacial potential at the solvent/gate-oxide interface. The reference potential is the voltage applied at the gate electrode which is usually 0V (grounded reference electrode). The interface potential at the solvent/gate-oxide interface is determined by the surface dipole potential of the solution χ_{sol}, which is a constant, and the surface potential ψ_0, which is a chemical input parameter, usually governed by the solvent pH. Hence the expression for the ISFET flat band voltage becomes [9]:

$$V_{FB} = E_{ref} - \Psi_0 + \chi_{sol} - \frac{\Phi_{Si}}{q} - \frac{Q_{ss} + Q_{ox}}{C_{ox}} \qquad (2.4)$$

From equation (2.4) it can be seen all terms are constant except for the surface potential ψ_0. It is this term which makes the ISFET sensitive to the solvent pH. In other words, the drain current I_d of an ISFET is a unique function of the solvent pH.

The ISFET is primarily used as a pH sensor. With a properly chosen gate oxide material and a biomaterial layer (ion-selective layer) outside the gate oxide, ISFET can also measure the concentration of certain biomolecules in the electrolyte, such as protein, enzyme and DNA [3]. It was regarded as a low-cost alternative to traditional chemical sensors with potential for on-chip integration. However, several disadvantages, such as lack of good solid state electrodes, parasitic sensitivity to temperature and light, time dependent instability of sensor parameters, have restrained the development of ISFET as a popular biosensor technology [3].

7

2.1.2   Scaling of MOSFET

Over the past decades, the MOSFET has continually been scaled down in size. Starting with gate lengths of 10μm in 1970, currently Intel Corporation has reached 45 nm technology which contains transistors with a physical gate length of ~ 22 nm.

Scaling of MOSFET is desirable for several reasons. First, for a given chip area, more and more MOSFETs can be placed. Thus, same functionality can be realized in a smaller area, or chips can have more functionality in the same area. The fabrication costs for a semiconductor wafer are relatively fixed. Therefore the cost per chip is mainly determined by the number of chips produced per wafer. Hence, smaller MOSFET allows more chips per wafer, reducing the price per chip. Over the past 30 years the number of MOSFETs per chip has doubled approximately every two years. This doubling of the transistor number was first observed by Gordon Moore in 1965 and is commonly referred to as Moore's law [10]. Second, smaller MOSFET switches faster and consumes less power. For example, one scaling approach is to scale down the main device dimensions (including transistor length, width, and the oxide thickness) and the operating voltage with a factor of α (α<1). In this way, the transistor channel resistance is kept constant while gate capacitance is reduced by a factor of α. Therefore, the RC delay of the transistor scales with a factor of α. Also, the power consumed by each transistor decreases with a factor of α^2.

However, as the dimensions of MOSFET approach the nanometer regime (<100nm), we start seeing new effects arising from new physical phenomenon which impose difficult challenges in device design and fabrication. For example, due to the diffraction limit of light, the conventional lithography techniques used to fabricate MOSFET circuits will have difficulty to indefinitely reduce the transistor size or increase the transistor density. As stated by the United

States Semiconductor Industry Association, a nonprofit organization that estimates the technology requirements for future semiconductor industry and publishes the International Technology Roadmap for Semiconductors, it will be an arduous challenge to advance CMOS technology beyond the 22nm technology generation [11].

Stimulated by this challenge, extensive research has been conducted to look for possible solutions to overcome the scaling limit. Most of these technology improvements and innovations are based on new materials, such as strained Si channels [12], high-k gate dielectric [13, 14], metal gates [14], as well as on novel device designs, such as ultra thin body (UTB) transistors [15], FinFETs [16], Dual-Gate transistors [16] and Tri-gate transistors [17]. However, these technologies rely on an improvement of individual device performance parameter (such as increased carrier mobility, lower leakage current, or higher drive current) [18, 19] and cannot solve the problem the transistor size and density limitations.

2.1.3   Silicon nanowire

To directly address the scaling challenge, semiconducting nanowires, such as silicon nanowires, germanium nanowires, and GaAs nanowires, have been thoroughly investigated because of their compatibility with today's microelectronics industry and their potential in replacing conventional planar MOSFET structures. Semiconducting nanowires are cylindrical single crystal structures with a diameter of a few nanometers and length around several hundred nanometers. Because of their small diameters and highly confined nature, semiconducting nanowires exhibit several interesting and novel properties, such as high intrinsic mobility [20, 21] and enhanced phonon drag [22]. Also, semiconducting nanowires do not have density limitations since they are not fabricated using conventional lithography techniques. These advantages offer

possible way to the ultimate scaling of MOSFET using Gate-All-Around (GAA) structures.

Among several types of semiconducting nanowires, silicon nanowires (SiNWs) are the most popular one because they can be easily synthesize and doped, and the silion/silicon-oxide interface in very stable.

There are two popular techniques to synthesize SiNWs, one is the materials method known as vapor-liquid-solid (VLS) growth [23, 24], and the other is the templating method known as superlattice nanowire pattern transfer (SNAP) [25].

The VLS technique uses well-defined Au nanoclusters as catalysts and silane (SiH4) as the vapor-phase reactant. The Au nanoclusters are heated in the presence of vapor-phase silane to 362 ℃, a temperature of Au-Si eutectic, resulting in the formation of liquid droplet of Au-Si alloy. The droplet supersaturates in Si under a continuous flow of vapor silane, resulting in a continuous grwoth of solid silicon. The diameters of the SiNWs are determined by the dimension of Au nanoclusters. The length of the SiNWs can be controlled by turning off the silane source. The VLS technique can produce numerous SiNWs at one time with various doping configurations [26]. Also, the SiNWs can be grown on different substrates [27]. However, the VLS process has some disadvantages. One major problem is the doping level cannot be precisely controlled. The VLS doping is done in situ by adding dopant precursor to the reaction, producing SiNWs with doping levels and electrical properties with large variations. Additionally, the distribution of these SiNWs cannot be controlled since the location of synthesized SiNWs depends on the randomly distributed Au nanoclusters.

The SNAP uses molecular beam epitaxy (MBE) to create a physical template for nanowire patterning. Such template is a GaAs/$Al_xGa_{(1-x)}$As superlattice structure consisting of the alternating gallium-arsenide and aluminum-gallium-arsenide layers grown on top of a (100)

GaAs substrate. The GaAs layers are selectively etched to form a comb-like structure. The thickness of the AlGaAs layer will determine the NW width, while the GaAs thickness will determine the distance between the NWs. A platinum layer is then deposited with a tilted angle along the ridges of the AlGaAs layers to form platinum NWs. The metal-coated edge of the master is then positioned on the top of an epoxy-coated SOI wafer to transfer the platinum NWs onto the SOI surface [25]. The platinum NWs are released by etching the AlGaAs layers. Finally a Reactive ion etching (RIE) is applied to transfers the Pt NW pattern into the underlying silicon film. The doping level of the SiNWs can be adjusted using spin-on doping method (SOD). The SNAP technique allows reproducible fabrication of high-density SiNW arrays with precise control over the diameter, length, pitch and doping level. SiNWs have been fabricated using this technique with SiNW widths down to 8nm and full-width pitches down to 16nm [25]. Each SiNW can be as long as several millimeters. Also, SiNW arrays containing up to 1400 SiNWs have been fabricated.

Several attempts to fabricate discrete SiNW transistors using both back gate [28, 29] and GAA [30-32] device structures have been demonstrated. Figure 2.2 shows a SiNW FET with GAA structure [33]. The doped SNW core is enveloped by a silicon oxide layer and then a gate electrode. The source and drain extension of the SNW is doped with an opposite doping type. This device configuration is similar to the MOSFET structure. Experimental results showed that SiNW FET exhibited higher hole mobility, higher transconductance, more ideal subthreshold behavior, better gate control and better short channel performance than traditional planar MOSFETs.

SiNWs can be doped to be n or p type using a diffusion doping process and both n-doped SiNW FETs and p-doped SiNW FETs can be fabricated simultaneously on the same substrate. Individual p-doped SiNW FETs exhibited excellent performance compared to n-doped SiNW

11

FET, including high on/off ratios, low off currents, high mobilities, and low subthreshold swings. Thus, the p-doped SiNW is more popular than n-doped SiNW.
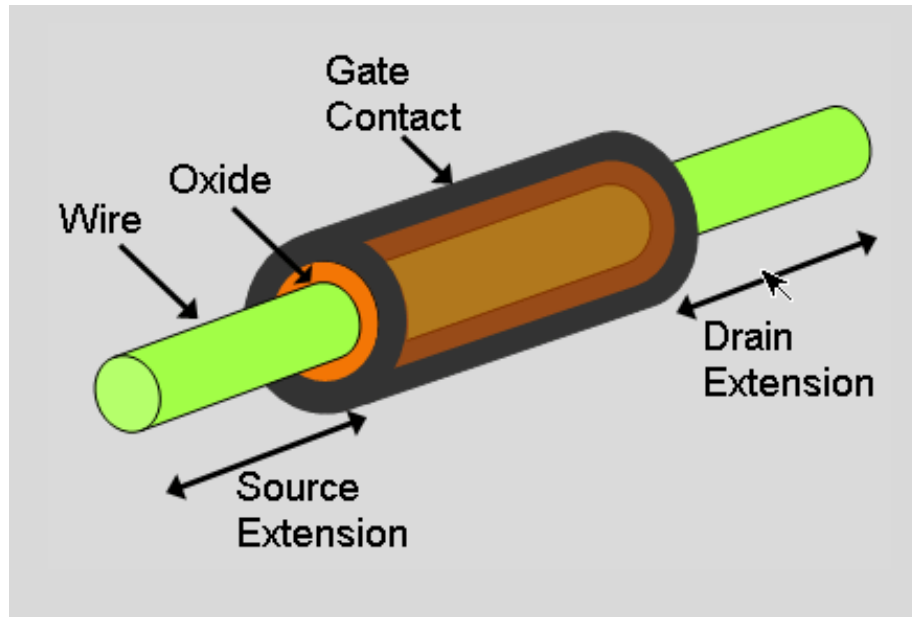
Figure 2.2 Scheme of a SiNW FET with GAA structure

2.1.4 Silicon nanowire sensor

The detection of biological and chemical species is gaining importance due to their large potential in commercial applications, ranging from diagnosing disease to discovery and screening of new drug molecules [1]. Biosensors based on SiNWs offer new and sometimes unique opportunities in this rich and interdisciplinary area of science and technology.

The configuration and the underlying detection mechanism of SiNW biosensor are similar to that of a SiNW FET. A SiNW FET, whose conductance is modulated by an applied gate voltage, is transformed into a biosensor by modifying the silicon oxide surface with a layer of biomaterial, and surface receptor biomolecules. The binding of a charged biomolecules (target biomolecules) to the gate dielectric is analogous to applying a voltage using a gate electrode. For example,

binding of a protein molecule with net negative charge to the surface of a p type SiNW will lead to an accumulation of positive hole carriers and increase the device conductance.

The SiNW FET biosensor overcomes limitations of ISFET sensor because of the one-dimensional morphology and large surface-to-volume ratio of the SiNW. The nanometer-scale cross-section of the SiNW leads to depletion or accumulation of carriers in the bulk of the device when a charged biomolecule binds to the SiNW surface (versus only the carriers at surface region will be modulated for an ISFET sensor). This unique feature of SiNW can promise sufficient sensitivity to detect single particle [34].

Nowadays, the protein detection methods can be divided into two general categories: label detection and label-free detection. Typical label-based methods involve detection of fluorescence, chemiluminescence or radioactivity from a specific label following target-receptor binding, and include the enzyme-linked immunosorbent assay (ELISA) [35] and nanoparticle labeling assay [36]. The label-based methods can detect biomolecules at relatively low concentrations. However, expensive and time-consuming preprocessing and postprocessing for sample preparation and data analysis are required in label-based detection. Thus, label-based methods are not suitable for real-time detection. The essential requirement for protein detection using a SiNW FET is a change in charge at the SiNW surface associated with binding and/or dissociation of analyte molecules. The change of charge distribution will modulate the carriers inside the SiNW and hence the drain current. This detection process is electronic rather than chemical. Thus no label and time-consuming sample preparation are required.

SiNW FET biosensors have already demonstrated real-time, label-free and highly sensitive detection of a wide range of species, including DNA, proteins, virus, pH levels, etc. Also, it is possible that arrays of SiNW FET biosensors will be able to detect a huge class of biomolecules.

13

The first example of detecting proteins in solution using SiNW FET biosensor is the detection of biotin/streptavidin binding. In this experiment, the oxide surface of the SiNW is modified with biotin molecules, which can bind with high selectivity to the protein streptavidin. When solutions of streptavidin are delivered to biotin modified SiNW, the conductance increases rapidly to a constant value, and the conductance value is maintained after the addition of pure buffer solution. These results can be explained with the net negative charge on streptavidin at the pH of these experiments (which will cause accumulation of holes in p type SiNW) and the very small dissociation rate of the biotin/streptavidin system.

The detection of biotin/streptavidin (or avidin) binding is of special interest and is widely demonstrated as a model system to study biorecognition between proteins and other biomolecules. The biotin/streptavidin system, with a binding affinity of 10^{15} M^{-1} for free complexes, exhibits one of the strongest noncovalent biological interactions known in nature. This binding couple remains highly stable under various harsh conditions, including extreme pH, salt concentration, and temperature. Biomolecules such as proteins and DNA can be easily biotinylated and bound to streptavidin coated surfaces.

Despite these promising experimental results of SiNW FET biosensors and their enormous potential in commercial applications, it is somewhat surprising that the fundamental mechanism of electrical sensing of biomolecules and the design principles of SiNW FET biosensor remain poorly understood. Many parameters affect the performance of SiNW FET biosensor, such as the dimension of the SiNW, the doping density of the SiNW, the surrounding environment (the ions concentration in the solvent). These parameters need to be investigated for the systematic optimization of biosensor design.

14

2.2   POISSON-BOLTZMANN EQUATION

Because of the long-range nature of Coulombic interactions [37], electrostatics plays a fundamental role in virtually all interactions involving biomolecules in ionic solution [38]. Continuum models of molecules in ionic solutions, first proposed in 1923 by Debye and Hückel [39], are important tools for studying electrostatic interactions in the ionic solution. The Poisson-Boltzmann equation is the fundamental equation arising in the Debye-Hückel theory. It is a three dimensional second order nonlinear elliptic partial differential equation describing the electrostatic potential $\Phi(r)$ at position r. In this chapter, the Poisson-Boltzmann equation is derived from the classical Poisson equation using the Boltzmann distribution to model the charge distribution in the ionic solution. Then some of the methods used to solve the equation are introduced.

2.2.1   Gauss's law

In physics, Gauss's law is a law relating the distribution of electric charge to the resulting electric field. In free space or vacuum, Gauss's law may be expressed in its differential form:

$$\nabla \cdot \vec{E} = \frac{\rho}{\varepsilon_0} \quad (2.5)$$

where $\nabla \cdot$ denotes divergence, $\vec{E}$ is the electric field, and ρ is the total electric charge density (including both free and bound charge), and ε_0 is the permittivity in vacuum. Using the relation:

$$\vec{E} = -\nabla\Phi \quad (2.6)$$

where Φ is the scalar potential and ∇ denotes gradient operation, equation (2.5) can be rewritten as:

$$\nabla \cdot \nabla \Phi = \nabla^2 \Phi = -\frac{\rho}{\varepsilon_0} \quad (2.7)$$

This equation is called Poisson equation. In region of space that lacks a charge density, equation becomes Laplace equation:

$$\nabla^2 \Phi = 0 \quad (2.8)$$

In a dielectric, the differential form of Gauss' law is then given by the following equations:

$$\nabla \cdot \vec{D} = \rho \quad (2.9)$$

$$\vec{D} = \varepsilon_0 \vec{E} + \vec{P} \quad (2.10)$$

where $\vec{D}$ is electric displacement vector, $\vec{P}$ is the polarization vector. In linear dielectric, the polarization $\vec{P}$ becomes zero, and equation (2.9) becomes:

$$\vec{D} = \varepsilon_0 \vec{E} \quad (2.11)$$

The dielectric constant or relative permittivity, ε_r, is defined as the ratio of the permittivity in the dielectric, ε, to the permittivity in vacuum, ε_0:

$$\varepsilon_r = \frac{\varepsilon}{\varepsilon_0} \quad (2.12)$$

Finally, the differential form of Gauss' law for a linear dielectric can be written as:

$$-\nabla \cdot (\varepsilon \nabla \Phi) = \rho \quad (2.13)$$

A detailed derivation of the Gauss' law in both free space and in a dielectric can be found in [40].

2.2.2 Boltzmann distribution

In physics, the Boltzmann distribution is a certain distribution or probability measure of a system of particles among the various energy states. For a system of N ($N = \sum_i n_i$) particles, the Boltzmann distribution gives the most probable distribution of finding n_1 particles with energy u_1, n_2 particles with energy u_2, and so on.

The Boltzmann distribution can be derived using the assumption of distinguishable particles. Suppose we have a number of energy levels, labeled by index i (i=1, 2,...k), each energy level having energy u_i and containing n_i particles. We use **W** to denote the number of ways of distributing n_i particles with energy u_i. In this derivation, we ignore the degeneracy problem, that means, there is only one way to put n_i particles into energy level i. We can distribute N particles in the following orders: selecting n_1 particles from N particles and placing them in energy level 1; then selecting n_2 particles from remaining N-n_1 particles and placing them in energy level 2; continuing this process until all particles are distributed. It can be easily seen that the number of ways of selecting n_1 objects from N objects without regard to order is:

$$C_N^{n_1} = \frac{N!}{n_1!(N-n_1)!} \quad (2.14)$$

Similarly, the number of ways of selecting n_2 objects from N-n_1 particles without regard to order is:

$$C_{N-n_1}^{n_2} = \frac{(N-n_1)!}{n_2!(N-n_1-n_2)!} \quad (2.15)$$

So **W** can be calculated as:

$$W = C_N^{n_1} C_{N-n_1}^{n_2} ... C_{n_k}^{n_k} = (\frac{N!}{n_1!(N-n_1)!})(\frac{(N-n_1)!}{n_2!(N-n_1-n_2)!})...(\frac{n_k!}{n_k!0!}) = \frac{N!}{n_1!n_2!...n_k!} \quad (2.16)$$

We wish to find a set of n_i to maximize W subject to the constraint that the number of particles and energy level are fixed. Since maxima of W and $\ln(W)$ can be obtained by the same value of n_i, for simplicity in mathematics, we will maximize $\ln(W)$ instead of maximizing W. To maximize $\ln(W)$ subject to the constraint of the number of particles and energy level, we construct a function using the method of Lagrange multipliers:

$$f(n_1, n_2, ... n_k) = \ln(W) + \alpha(N - \sum_i n_i) + \beta(E - \sum_i n_i u_i) \quad (2.17)$$

where the last term on the right hand side shows the conservation of total energy.

From equation (2.16), we can get

$$\ln W = \ln(N!) - \sum_i \ln(n_i!) + \sum_i (n_i \ln g_i) \quad (2.18)$$

Using Stirling's formula [41], for large N,

$$N! \approx N^N e^{-N} \quad (2.19)$$

we can get

$$\ln(N!) \approx N \ln N - N \quad (2.20)$$

also noticing that $N = \sum_i n_i$, then we can get

$$\ln W = N \ln N - \sum_i (n_i \ln n_i) + \sum_i (n_i \ln g_i) \quad (2.21)$$

finally

$$f(n_1, n_2, ... n_k) = N \ln N + \alpha N + \beta E + \sum_i (n_i \ln g_i - n_i \ln n_i - (\alpha + \beta \mu_i) n_i) \quad (2.22)$$

In order to maximize the above equitation, the partial derivative of function f with respect to n_i should be zero:

$$\frac{\partial f}{\partial n_i} = \ln g_i - \ln n_i - (\alpha + \beta \mu_i) = 0 \quad (2.23)$$

By solving the above equation, and noticing thermodynamically that $\beta = \dfrac{1}{K_B T}$ where

K_B is the Boltzmann's constant and *T* is the absolute temperature of the system, we can get the

expression for n_i :

$$n_i = n_\infty \exp(-\frac{u_i}{K_B T}) \quad (2.24)$$

This is the well known Boltzmann distribution. Here, n_∞ is the mean distribution at far-

field [42]. More details on the derivation of the Boltzmann distribution can be found in [43] and

[44].

2.2.3   Poisson-Boltzmann equation

Figure 2.3 shows an ionic solvent model which contains a kind of biological molecules

(typically proteins, DNA, RNA and other biomolecules) and electrolytic ions such as Na^+, K^+,

Ca^+, Mg^+, Cl^-. In this model, the biomolecule is located in region Ω_1 . Region Ω_2 is an exclusion

layer around the biomolecule in which no mobile ions of the solvent are present. Region Ω_3

consists of the solvent which contains electrolytic ions. Region Ω_2 has the same dielectric

constant as in region Ω_3 ($\varepsilon_2 = \varepsilon_3$). The electrostatic potential $\Phi(r)$ satisfies Gauss' law in each of

the three regions. However, the charge density ρ , the right hand side term in equation (2.13), is

different for different regions.
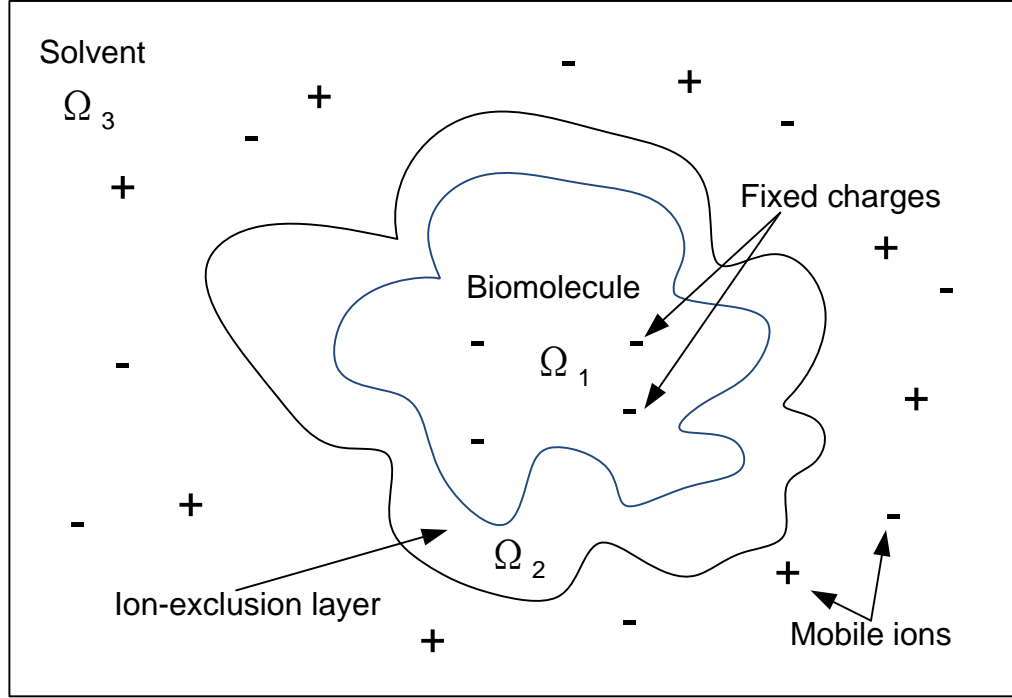
Figure 2.3 Two-dimensional view of the three-dimensional ionic solvent model

The biomolecule in region Ω_1 is composed with n atoms and has a set of fixed charges on its atoms. For example, the DNA molecule has a set of fixed negative charges due to the phosphate backbone of the DNA chain. The electrolytic ions in region Ω_3 are mobile and diffuse. To achieve charge distribution equilibrium, counterions in the solution will surround the biomolecule. In the case of DNA, the DNA molecule will be surrounded by positive ions such as Na^+, K^+, Ca^+, Mg^+. The distribution of the mobile ions in region Ω_3 can be characterized using Boltzmann distribution and the energy at any point in the solution is given by the electrostatic energy of the ions at that point.

Now let's consider Gauss' law in each of the three regions. In region Ω_1, the fixed charges can be modeled using delta function:

$$\rho_{fixed} = q \sum_{i}^{N} z_i \delta(r - r_i) \quad (2.25)$$

where q is the elementary charge, N is the number of fixed charges present, , z_i and r_i are their charges and positions, and $\delta(r)$ is the Dirac delta function. The Gauss' law in region Ω_1 becomes

$$-\nabla \cdot (\varepsilon_0 \varepsilon_1 \nabla \Phi_1(r)) = q \sum_i^N z_i \delta(r - r_i) \quad (2.26)$$

In region Ω_2, the charge density function equals to zero due to the absence of mobile ions in the exclusion layer. The Gauss' law in region Ω_2 becomes

$$-\nabla \cdot (\varepsilon_0 \varepsilon_2 \nabla \Phi_2(r)) = 0 \quad (2.27)$$

In region Ω_3, the charge density distribution ρ is due to the mobile ions in the solution. The distribution of mobile charges can be described using Boltzmann distribution

$$\rho_{mobile} = \sum_j^{N_{ions}} q z_j n_\infty \exp(\frac{-qz_j \Phi}{K_B T}) \quad (2.28)$$

where N_{ions} is the number of the mobile ions, z_j is the charge of the ion, n_∞ is the concentration of the ion at a distance of infinity from the solute and Φ is the electrical potential. The Gauss' law in region Ω_3 then becomes

$$\nabla \cdot (\varepsilon_0 \varepsilon_3 \nabla \Phi_3(r)) = -\sum_j^{N_{ions}} q z_j n_\infty \exp(\frac{-qz_j \Phi(r)}{K_B T}) \quad (2.29)$$

Physically, the electrostatic potential function $\Phi(r)$ should be continuous at the interface of the regions. In particular, at the interface of region Ω_1 and region Ω_2, it must be true that $\Phi_1(r) = \Phi_2(r)$. While at the interface of region Ω_2 and region Ω_3, it must be true that $\Phi_2(r) = \Phi_3(r)$. Also, for the infinite domain, the electrostatic potential at infinite far should be zero, i.e., $\Phi(\infty) = 0$.

We now define the piecewise dielectric constant function $\varepsilon(r)$ and a parameter $\alpha(r)$ on the whole domain $\Omega = \Omega_1 \cup \Omega_2 \cup \Omega_3$,

$$\varepsilon(r) = \begin{cases} \varepsilon_1, r \in \Omega_1 \\ \varepsilon_2(=\varepsilon_3), r \in \Omega_2 \text{ or } \Omega_3 \end{cases} \qquad \alpha(r) = \begin{cases} 0, r \in \Omega_1 \text{ or } \Omega_2 \\ 1, r \in \Omega_3 \end{cases} \qquad (2.30)$$

Now we can write a single equation governing the electrostatic potential $\Phi(r)$ in all the three regions:

$$\nabla \cdot (\varepsilon_0 \varepsilon(r) \nabla \Phi(r)) = -q \sum_i^N z_i \delta(r - r_i) - \alpha(r) \sum_j^{N_{ions}} q z_j n_\infty \exp(\frac{-q z_j \Phi(r)}{K_B T}) \qquad (2.31)$$

For a solvent only contains two types of ions with charges of $+q$ and $-q$, respectively, the above equation can be reduced to a nonlinear elliptic partial differential equation known as nonlinear Poisson-Boltzmann equation:

$$-\varepsilon_0 \nabla \cdot (\varepsilon(r) \nabla \Phi(r)) + 2\alpha(r) q n_\infty \sinh(\frac{q\Phi(r)}{K_B T}) = q \sum_i^N z_i \delta(r - r_i) \qquad (2.32)$$

or

$$-\nabla \cdot (\varepsilon(r) \nabla \Phi(r)) + \frac{\varepsilon_3 \kappa^2 K_B T \alpha}{q} \sinh(\frac{q\Phi(r)}{K_B T}) = \frac{q}{\varepsilon_0} \sum_i^N z_i \delta(r - r_i) \qquad (2.33)$$

where

$$\kappa = \sqrt{\frac{2 n_\infty q^2}{K_B T \varepsilon_3 \varepsilon_0}} \qquad (2.34)$$

κ is the Debye- Hückel screening parameter. κ^{-1} is called the Debye screening length, it is an important parameter to characterize the thickness of the ion atmosphere, which is an electrical double layer. This will be discussed in the later chapter.

n_∞ can be expressed in terms of I_s, the ionic strength of the solvent

$$n_\infty = N_A I_s \qquad (2.35)$$

22

where N_A is the Avogadro number and

$$I_s = \frac{1}{2}\sum_{i=1}^{N_i} c_i z_i^2 \quad (2.36)$$

where c_i is the molar concentration of ion i (mol/cm^3). Equation (2.34) and (2.35) clearly shows

the dependence of κ on the ionic strength of the solvent.

When the electrostatic potential $\Phi(r)$ is very small, we can use the first term in the Taylor

series expansion $\sinh x = x + \frac{x^3}{3!} + \frac{x^5}{5!} + ...$ as a linear approximation to $\sinh(\frac{q\Phi(r)}{K_B T})$, and equation

(2.33) can be linearized as

$$-\nabla \cdot (\varepsilon(r)\nabla\Phi(r)) + \varepsilon_3 \kappa^2 \alpha \Phi(r) = \frac{q}{\varepsilon_0}\sum_i^N z_i \delta(r - r_i) \quad (2.37)$$

which is called linearized Poisson-Boltzmann equation. The linearized Poisson-Boltzmann

equation is applicable for highly charged molecules like DNA as the magnitude of the

electrostatic potential is no longer very small.

2.2.4   Solution of the Poisson-Boltzmann equation

In the Poisson-Boltzmann equation, the dielectric constant function $\varepsilon(r)$ varies by more than

an order of magnitude across the interface between the biomolecule and surrounding solvent.

Usually, the dielectric constant of the biomolecule is around 2-20 and the dielectric constant of

the solvent is around 80 (the dielectric constant of water). The Debye-Hückel screening

parameter κ, proportional to the ionic strength of the solution, is discontinuous at the interface

between the solvent region and the ion exclusion layer surrounding the biomolecular surface.

The fixed charges of the biomolecule yields a delta function, which is difficult to deal with. In

general, the Poisson-Boltzmann equation can only be solved using computational methods due to the rapid exponential nonlinearities, discontinuous coefficients, delta functions, and infinite domain. And the accuracy and stability of the solution to the Poisson-Boltzmann equation is quite sensitive to the boundary layer between the solvent and the ion exclusion layer which defines the solvent-accessible surface.

2.2.4.1 Analytical solutions of the Poisson-Boltzmann equation

In special cases, analytical solutions to the linearized Poisson-Boltzmann equation can be explicitly constructed separately in different regions and then brought together by making sure continuity conditions at the region boundaries.

Spherical molecule with uniform charge

Let's consider the model shown in Figure 2.4, a spherical biomolecule is immersed in a solvent which contains mobile univalent ions. Total fixed charge q is assumed to be evenly distributed on the molecule surface. The system coordinate is defined to be centered at the molecule. The radius of the biomolecule is denoted by R, which defines region Ω_1. The thickness of the ion exclusion layer, region Ω_2, is denoted by *a-R*. The ionic solvent then lies in the region Ω_3, defined by r>a.

The charge q is evenly distributed over the biomolecule surface of area $4\pi R^2$, so the biomolecule has the uniform charge density:

$$\sigma = \frac{q}{4\pi R^2} \quad (2.38)$$

The linearized form of the Poisson-Boltzmann equation in spherical coordinates with spherical symmetry can be easily reduced to:

24

$$\text{region } \Omega_1 : \ -\frac{1}{r^2}\frac{d}{dr}(r^2\frac{d}{dr}\Phi(r)) = 0, \ \ r < R,$$

$$\text{region } \Omega_2 : \ -\frac{1}{r^2}\frac{d}{dr}(r^2\frac{d}{dr}\Phi(r)) = 0, \ \ R < r < a, \qquad (2.39)$$

$$\text{region } \Omega_3 : \ -\frac{1}{r^2}\frac{d}{dr}(r^2\frac{d}{dr}\Phi(r)) + \varepsilon_3\kappa^2\Phi(r) = 0, \ \ r > a,$$

$$\text{boundary condition}: \ \Phi(\infty) = 0,$$

where the zeros at the right hand side of the above equations are result from placing the fixed

charge q on the biomolecule surface.
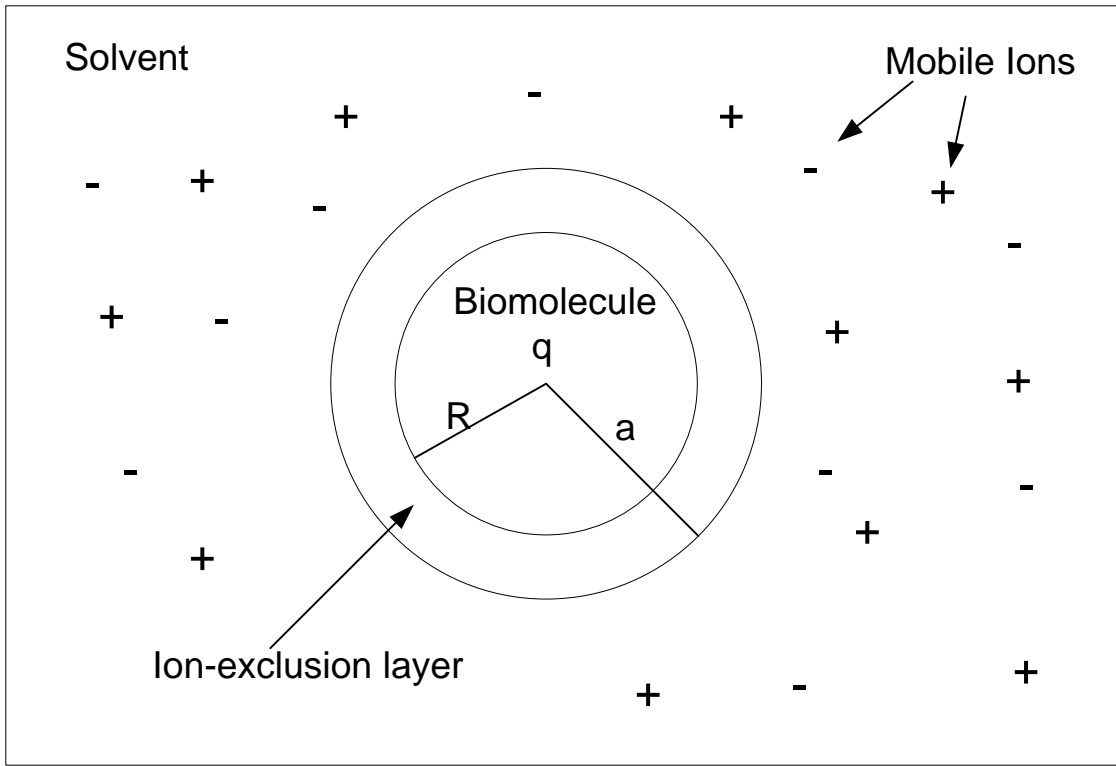
Figure 2.4 An ionic solvent model

The boundary conditions at the interface of region Ω_1 and region Ω_2 (at $r=R$) should satisfy:

$$\Phi_1(r) = \Phi_2(r)$$

$$\varepsilon_1(\frac{d\Phi_1}{dr}) - \varepsilon_2(\frac{d\Phi_2}{dr}) = -4\pi\sigma = \frac{-q}{R^2} \qquad (2.40)$$

The boundary conditions at the interface of region Ω_2 and region Ω_3 (at $r=a$) should satisfy:

$$\Phi_2(r) = \Phi_3(r)$$
$$\varepsilon_2 \left(\frac{d\Phi_2}{dr}\right) = \varepsilon_3 \left(\frac{d\Phi_3}{dr}\right) \quad (2.41)$$

By differentiating twice, the general solution in each region can be achieved as:

$$\text{region } \Omega_1 : \quad \Phi_1(r) = c_1 + \frac{c_2}{r}$$

$$\text{region } \Omega_2 : \quad \Phi_2(r) = c_3 + \frac{c_4}{r} \quad (2.42)$$

$$\text{region } \Omega_3 : \quad \Phi_3(r) = c_5 \frac{e^{-\kappa r \sqrt{\varepsilon_3}}}{r} + c_6 \frac{e^{\kappa r \sqrt{\varepsilon_3}}}{r}$$

The six constants can be calculated by applying the boundary and continuity conditions, and the requirement that $\Phi(r)$ be finite in region Ω_1. The resulting expressions for the electrostatic potential in each region are:

$$\text{region } \Omega_1 : \quad \Phi_1(r) = \frac{q}{\varepsilon_3 R}\left(1 - \frac{R\kappa\sqrt{\varepsilon_3}}{1 + \kappa a \sqrt{\varepsilon_3}}\right)$$

$$\text{region } \Omega_2 : \quad \Phi_2(r) = \frac{q}{\varepsilon_3 r}\left(1 - \frac{r\kappa\sqrt{\varepsilon_3}}{1 + \kappa a \sqrt{\varepsilon_3}}\right) \quad (2.43)$$

$$\text{region } \Omega_3 : \quad \Phi_3(r) = \frac{q e^{\kappa a \sqrt{\varepsilon_3}}}{\varepsilon_3 (1 + \kappa a \sqrt{\varepsilon_3})} \cdot \frac{e^{-\kappa r \sqrt{\varepsilon_3}}}{r}$$

Infinite planar membrane-solvent system

As shown in Figure 2.5, an infinite planar membrane is immersed in the solvent. Assume the fixed charge on the membrane is evenly distributed at the interface of the membrane and the solvent. Then the Poisson-Boltzmann equation for this system can be solved analytically using an approach known as Gouy-Chapman theory. Gouy-Chapman theory is based on a continuum model for the membrane-solvent system [45].

26
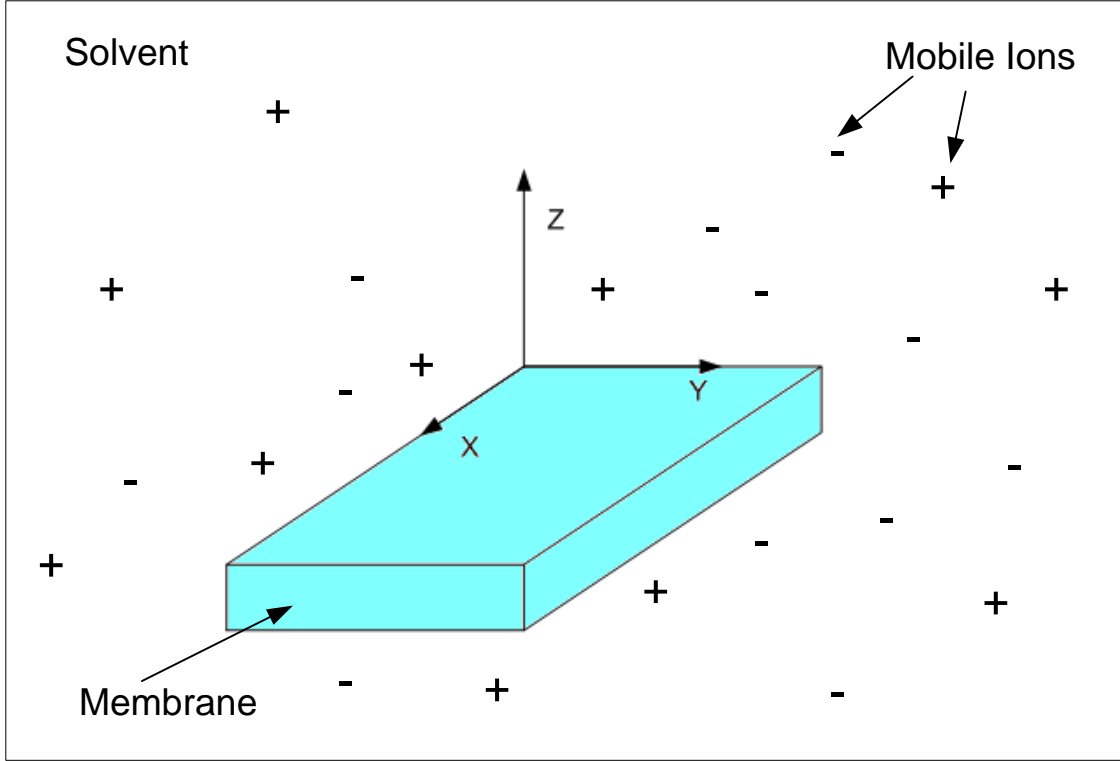
Figure 2.5 An infinite planar membrane-solvent system

The Poisson-Boltzmann equation for this system can be written as:

$$-\nabla \cdot (\varepsilon_0 \varepsilon_s(r) \nabla \Phi(r)) + \frac{\varepsilon_0 \varepsilon_s \kappa^2 K_B T}{q} \sinh(\frac{q\Phi(r)}{K_B T}) = 4\pi\rho \quad (2.44)$$

where ε_s is the dielectric constant in the solvent and ρ is the fixed charge density. The boundary condition is $\Phi(z) = 0$ when z approaches infinite.

There are several key assumptions in Gouy-Chapman theory which enable an analytic solution of equation (2.44). One is that the membrane is infinite and planar, so that the interface between the membrane and the solvent can be described as an infinite plane which separates two regions, each with a different dielectric constant. Another one is that the surface of the membrane is assumed to contain a constant fixed charge density ρ, with unit of charge per area.

Under these assumptions, the electrostatic potential in the solvent is dependent only on the distance z from the membrane surface. It is given by

27

$$\Phi(z) = \frac{4K_BT}{q} \tanh^{-1}[\exp(-kz)\tanh(\frac{q\Phi_0}{4K_BT})] \quad (2.45)$$

where Φ_0 is the electrostatic potential at the interface between the membrane and the solvent and it can be written as

$$\Phi_0 = \frac{2K_BT}{q} \sinh^{-1}(\frac{2\pi q\rho}{\varepsilon_0\varepsilon_s\kappa K_BT}) \quad (2.46)$$

2.2.4.2 Numerical solutions of the Poisson-Boltzmann equation

Finding efficient solvers to numerically solve the Poisson-Boltzmann equation for a large class of macromolecules has been an active area of research for over a decade now. In the current numerical methods, the biomolecular-solvent system is modeled by dielectrically distinct regions with singular charges distributed in the molecular region (fixed point charges in Poisson-Boltzmann equation). The biomolecular-solvent system is then discretized and represented as a distribution of points and their connections. The generation of this presentation, called mesh generation, is generally a difficult task since it is always complicated by the identification of the irregular molecular surface and an appropriate description of this surface for resolving the molecular structure in sufficient details. The fineness of the mesh is critical to the efficiency and accuracy of the numerical methods. A coarser mesh results in higher efficiency but lower accuracy, and vice versa. Once the molecular surface is identified and discretized, the remaining procedure depends on the particular numerical method adopted.

Finite difference method [46], boundary element method [47] and finite element method [48] are among the most popular numerical methods.

Finite difference method has been the most popular numerical method for the Poisson-Boltzmann equation because of its simple implementation since mesh generation and refinement

are trivial for finite difference method. DelPhi [49], GRASP [50], MEAD [51], UHBD [52], and the PBEQ [53] module in CHARMM [54] are among the most successful finite difference based Poisson-Boltzmann equation for computing biomolecular electrostatics. The major disadvantages in applying the finite difference method to numerically solve the Poisson-Boltzmann equation are the large number of unknowns and the low efficiency of linear solvers in general. Two methods can be used to remedy these problems. The first one is to use fine mesh near the active sites on the molecular surface and coarse mesh in the solvent region far away from the molecules. The second one is to use a very coarse mesh in the entire domain to obtain a rough potential distribution first and then use a finer mesh in the interesting region to solve the Poisson-Boltzmann equation locally with boundary conditions interpolated from the results on coarse mesh.

Boundary element method invokes Green's theorem to change the linear Poisson-Boltzmann differential equations as certain boundary integral equation. Thus, the unknowns and the mesh generation are only on a 2D surface [55]. The advantages of boundary element method are: the number of unknowns is reduced significantly; compared with finite difference method where the jump boundary condition is smoothed by the interpolation scheme instead of being enforced, the physical interface conditions on the molecular surface are explicitly treated thus the solution on the interface is more accurate; the singular charges distributed within the biomolecules can be analytically treated. The disadvantages of boundary element method are: this method is only applicable to the linear Poisson-Boltzmann equation since no Green's functions are available for the nonlinear Poisson-Boltzmann equation; the efficiency is not very good because numerous boundary integral operations are required; the accuracy and stability are affected by singular boundary integrals.

Finite element method, compared with the finite difference method and boundary element method, provides more flexibility for local mesh refinement, more rigorous convergence analysis and more choices of efficient iterative solvers for the linear Poisson-Boltzmann equation, and more flexibility for handling nonlinear Poisson-Boltzmann equation. The main disadvantage of finite element method is its inefficiency in dealing with the nonlinear problems. Also, efficient and accurate mesh generation for molecular surface is still required to make this method popular.

Some hybrid methods are used to improve the efficiency and accuracy of the methods mentioned above. For example, parallel implementations and use of fast solvers like multi-grid and domain decomposition are combined with finite difference method; fast multi-pole and precorrected FFT methods are combined with boundary element method; and adaptive multilevel methods are combined finite element method.

3.0   MODELING AND SIMULATION METHOD

3.1   THE STRUCTURE OF SINW FET BIOSENSOR

The structure of the SiNW FET biosensor is similar to that of SiNW FETs, except that the surface of the nanowire is functionalized with a layer of probe molecules which can only bind to a specific kind of target molecules in an aqueous solution. The general schematic of a SiNW FET biosensor is shown in Figure 3.1(a). A SiNW core is placed on silicon dioxide substrate with its two ends connected to two electrodes (source and drain). The SiNW core is enveloped by a silicon-oxide layer whose surface is functionalized with specific receptor molecules (green) which recognize and bind only to the target molecules (red). The SiNW is immersed in the electrolyte which contains target molecules, Na^+ and Cl^- ions.

Electrolyte is used as buffer solution which resists pH change upon addition of small amount of acid or base, or upon dilution. The target molecules are randomly distributed in the electrolyte and they diffuse through the solution and reach the SiNW and get captured by the receptor molecules, binding the receptor molecules close to the silicon oxide surface. Many biomolecules carry charges under the normal physiological conditions. For example, DNA carry negative charges whereas the net charges of protein depend on the pH value of the electrolyte. The charges of the bound target molecules interact with the charge in the SiNW and modulate the

31

conductance of the SiNW. A back gate electrode U_{BG} and a reference electrode U_G are connected to the system to adjust the bulk electrolyte potential.
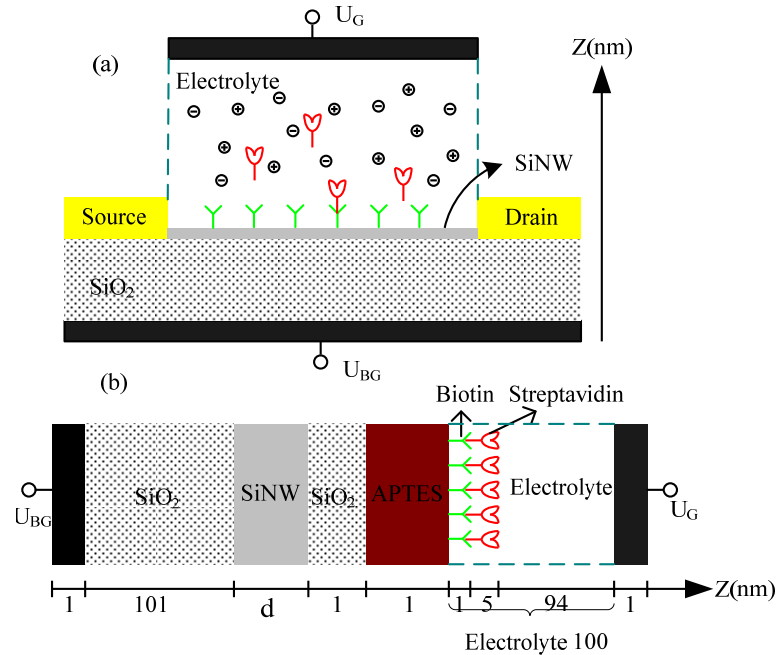
Figure 3.1 General schematic of SiNW FET biosensor (a) General schematic of SiNW FET biosensor. The surface of SiNW is functionalized with receptors (green) for target biomolecules (red). (b) Structure SiNW FET biosensor for detection of biotin/streptavidin binding between the source and drain region along Z axis. On the surface of SiNW there is a native oxide which is covalently bound to a layer of APTES molecules. And biotin molecules are chemically attached to the APTES surface. The biosensor is immersed in aqueous solution to detect streptavidin in the solution. The numbers denote dimension of various layers along Z axis.

The structure SiNW FET biosensor for detection of biotin/streptavidin binding is slightly different from the structure of general SiNW FET biosensor. The biotin molecules cannot be directly immobilized on the silicon oxide surface. A layer of aminopropyltriethoxysilane (APTES) molecules are covalently bound to the silicon oxide surface. And biotin molecules (receptor molecules) are chemically attached to the APTES surface. The streptavidin molecules in aqueous solution can be specifically bound to biotin molecules. Figure 3.1(b) shows the cross-section view of the SiNW FET biosensor along Z axis. Here we assume the thickness of the

32

silicon oxide substrate is 100nm, the thickness of the silicon oxide layer enveloping the SiNW core is 1nm, the thickness of APTES molecules layer is 1nm. The dimension of biotin molecule and streptavidin molecule are 0.52nm×l.00nm×2.10nm and 4.5nm×4.5nm×5.0nm, respectively. So we model the biotin and steptavidin molecules as spheres and assume the thickness of biotin layer is 1nm and the thickness of streptavidin is 5nm. The electrolyte (NaCl solution with various concentration, the pH value is assumed as 7) region is 100nm and the thickness of metal electrode is 1nm. The length, diameter (denoted as d) and the doping density (assume a p-type doping) of the SiNW are variable.

3.2   THEORETICAL APPROACH

To detect the biotin/Streptavidin binding in the electrolyte, generally two states of the SiNW FET biosensor should be simulated. In the first state only the receptor molecules (biotin) are attached to the APTES layer surface. In the second state, the target biomolecules (streptavidin) are attached to the biotin surface due to specific binding. The change of charge distribution arising from the biotin/streptavidin binding modulates the electrostatic potential on the silicon oxide surface of the SiNW and hence modulates charge distribution inside the SiNW core. As a consequence, the current flows in the SiNW will be changed accordingly. The I-V characteristics of the SiNW can be examined to determine the sensitivity of the biosensor. The followings are some technical details.

Using the drift-diffusion charge transport model, the carrier transport in the SiNW core can be written as [56]:

$$J_{e,h} = q\mu_{e,h}n_{e,h}\nabla\Phi \pm qD_{e,h}\nabla n_{e,h} \quad (3.1)$$

33

where q is elementary charge ($q=1.6\times10^{-19}$C), J is the current density, μ is the mobility of the carriers, n is the carrier density, Φ is the electric potential, and D is the diffusion coefficient. The subscript e and h denote electron and hole, respectively. The relationship between the electrostatic potential and the carrier concentrations can be described using Poisson's equation:

$$-\nabla(\varepsilon_{Si}\nabla\Phi(r))=q(n_h-n_e+N_D-N_A) \quad (3.2)$$

where ε_{Si} is the dielectric constant of silicon, r is the spatial coordinate, and N_D and N_A are the donor and acceptor concentration within the SiNW, respectively. Here we assume the dopants are completely ionized.

In the silicon oxide layer, we assume that there is no defect in the native oxide and neglect any interface traps and fixed oxide charges. The electrostatic potential in the silicon oxide is given by the Poisson's equation:

$$-\nabla(\varepsilon_{Ox}\nabla\Phi(r))=0 \quad (3.3)$$

where ε_{ox} is the dielectric constant of silicon oxide.

The APTES molecules layer serves as a passivation layer and no charge carriers are assumed to be present within this layer. Similarly, the electrostatic potential in the APTES molecules layer is given by the Poisson's equation:

$$-\nabla(\varepsilon_{APTES}\nabla\Phi(r))=0 \quad (3.4)$$

where ε_{APTES} is the dielectric constant of APTES molecules layer.

In the SiNW MOSFETs, the gate voltage is externally applied via a gate electrode enveloping the silicon oxide layer. In the SiNW FET biosensor, no gate electrode is present and the gate voltage is determined by solving the nonlinear Poisson-Boltzman equation (NPBE) [57]:

$$-\nabla(\varepsilon_r(r)\nabla\Phi(r))=\rho_{fixed}(r)+\rho_{mobile}(r) \quad (3.5)$$

where ρ_{fixed} is the charge density in the biotin layer and the bounded streptavidin molecules. And ρ_{mobile} is the mobile ions in the electrolyte which account for the Debye screening effect. ε_r is the dielectric constant of electrolyte.

The fixed charge density ρ_{fixed} can be modeled using delta function:

$$\rho_{fixed} = q\sum_{i}^{N} z_i \delta(r - r_i) \qquad (3.6)$$

where N is the number of fixed charges present, z_i and r_i are their charges and positions, and $\delta(r)$ is the Dirac delta function.

The distribution of mobile charge density ρ_{mobile} can be described using Boltzmann distribution:

$$\rho_{mobile} = \sum_{j}^{N_{ions}} qz_j n_\infty \exp(\frac{-qz_j \Phi}{K_B T}) \qquad (3.7)$$

where N_{ions} is the number of the mobile ions, z_j is the charge of the ion, n_∞ is the concentration of the ion at a distance of infinity from the solute and Φ is the electrical potential. K_B is the Boltzmann's constant and T is the absolute temperature.

For the special case of a 1-1 electrolyte (e.g. Na^+-Cl^-) with bulk concentration n, ρ_{mobile} can be written as [45]

$$\rho_{mobile} = -\frac{K_B T}{q} \varepsilon_r \kappa^2 \sinh(\frac{q\Phi}{K_B T})$$
$$(3.8)$$

where

$$\kappa = \sqrt{\frac{2n_\infty q^2}{K_B T \varepsilon_3 \varepsilon_0}} \qquad (3.9)$$

κ is the Debye- Hückel screening parameter. κ^{-1} is called the Debye screening length, it is an important parameter to characterize the thickness of the ion atmosphere, which is an electrical double layer.

Physically, the electrostatic potential function $\Phi(r)$ should be continuous at the interface of the various layers. Also, for the infinite domain, the electrostatic potential at infinite far should be zero, i.e., $\Phi(\infty) = 0$. As long as we get the solution for the NPBE of equation (3.5), the electrostatic potential in other layers can be solved by applying the continuous condition. And finally we can get the current density inside the SiNW using equation (3.1).

3.3   SIMULATION METHODS

In general, the NPBE can only be solved using computational methods due to the rapid exponential nonlinearities, discontinuous coefficients, delta functions, and infinite domain. And the accuracy and stability of the solution to the NPBE is quite sensitive to the boundary layer between the electrolyte and the biomolecules which defines the solvent-accessible surface.

In this work, a nano device simulator nextnano[3] [58] is used to solve the NPBE and get the electrostatic potential value in electrolyte, APTES molecules layer and silicon oxide layer. The nextnano[3] uses Gouy-Chapman theory [45] to solve the NPBE for a one dimension planar Ion-selective field effect transistor (ISFET) biosensor [59]. There are several key assumptions in Gouy-Chapman theory. One is that the surface of the ISFET biosensor is infinite and planar, so that the interface between the biomolecules and the electrolyte can be described as an infinite plane which separates two regions, each with a different dielectric constant. Another one is that the surface of the ISFET biosensor is assumed to contain a constant fixed charge density ρ, with unit of charge per area. Under these assumptions, the electrostatic potential in the electrolyte is dependent only on the distance z from the membrane surface. For our SiNW FET biosensor, the electrostatic potential is dependent only on the distance r from the APTES molecules layer along

36

the radius direction of the SiNW. Thus, it is feasible to use nextnano[3] to solve the NPBE for our

SiNW FET biosensor. And the critical step is to calculate the interface charge density ρ, i.e., the

charge density in the biotin layer before and after the binding of streptavidin molecules.

The protein will carry net charge if the pH value of the electrolyte not equal to the isoelectric

point (pI) value of the protein. The protein net charge at a given pH value can be estimated using

the Henderson-Hasselbalch equation [60]

$$pH = pK_a + \log_{10} \frac{[A^-]}{[HA]} = pK_a + \log_{10} \frac{\alpha}{1-\alpha} \quad (3.10)$$

where α is the fractional dissociation of any ionizable group [60] and pK_a is referred as the acid

dissociation constant. In the charge determination procedure [61], the pK_a for each type of

ionizable group is assigned a magnitude. Knowledge of the amino acid sequence (or

composition) of a protein is then used to calculate the net charge. The protein net charge arising

from n_i ionizable groups of type i, $(Z_P)_i$, is given by [60]

$$(Z_p)_i = n_i z_i \alpha_i \quad (3.11)$$

if the ionizable group, i, is anionic (z_i is negative), or

$$(Z_p)_i = n_i z_i (1 - \alpha_i) \quad (3.12)$$

if the ionizable group, i, is cationic (z_i is positive). The pK_a value of biotin is 4.66 [62], so at

pH=7, each biotin molecule carry net charge of $\alpha=1/(1+10^{4.66-7})\approx-1q$. This result coincides with

the experimental result in [63].

The net charge of streptavidin is contributed by terminal amino acids and charged amino

acid side-chains within the protein sequence [64]. It can be determined by computer programs

given the protein sequence data and a set of pK_a values for proton dissociation from ionizable

groups [61]. We use a web based server H++ [65, 66] to calculate the net charge of streptavidin at pH=7. Given the atomic resolution Protein Data Bank (PDB) structures, the H++ can perform a quick estimate of pK_a values as well as the protein net charge at a specific PH value. The calculated net charge is +9q, which means a treptavidin molecule carries 9 positive elementary charges at pH value of 7. Based on the net charge of biotin and streptavidin molecule, along with the dimension information of the SiNW, we can estimate the interface charge density ρ within the biotin layer before and after the binding of streptavidin molecules.

Nextnano[3] needs the following parameters to calculate the electrostatic potential in electrolyte, APTES molecules layer and silicon oxide layer: the dimension information of various layers and electrolyte, the doping density of the SiNW, the ions (NaCl) concentration of the electrolyte, the interface charge density ρ and the voltages applied on electrodes U_{BG} and U_G. The dimension information of various layers and electrolyte is shown in figure 3.1(b). The interface charge density ρ can be calculated using the dimension information and the net charge of biotin/streptavidin. The voltages applied on electrodes U_{BG} and U_G are set to be zero. Now we are ready to calculate the electrostatic potential corresponding to different SiNW diameters, doping densities and ions concentrations of the electrolyte.

4.0   SIMULATION RESULTS AND DISCUSSION

We define the silicon oxide surface potential change $\Delta\Phi_s$ as

$$\Delta\Phi_s = \Phi_s(n) - \Phi_s^{ref} \qquad (4.1)$$

where n denotes the number of streptavidin molecules bound to the avidin molecules, Φ_s^{ref} is the reference voltage when no streptavidin molecules are bound to the avidin molecules.

For a SiNW with diameter d=10nm, doping density $p=10^{15}cm^{-3}$, length L=50nm, and the NaCl concentration in the electrolyte is 10mM. Assume the number of streptavidin molecules bound to the SiNW surface varies from 0 to 10, the calculated surface potential change $\Delta\Phi s$ is shown in Figure 4.1 (green line). As can be seen, the surface potential at the silicon oxide layer increases as the number of the bound streptavidin molecules increases. The curve is nonlinear due to the Debye screening effect of the electrolyte where the ions (Na^+, Cl^-) in the electrolyte screen the charges on the biotin and streptavidin molecules.

The Debye screening length, which is introduced in Chapter 4, is a critical parameter for label-free sensing using SiNW FET. The Debye screening lengths for different NaCl concentrations are shown in Table 1 and Figure 4.2. As can be seen, the screening length decreases as the NaCl concentration increases.
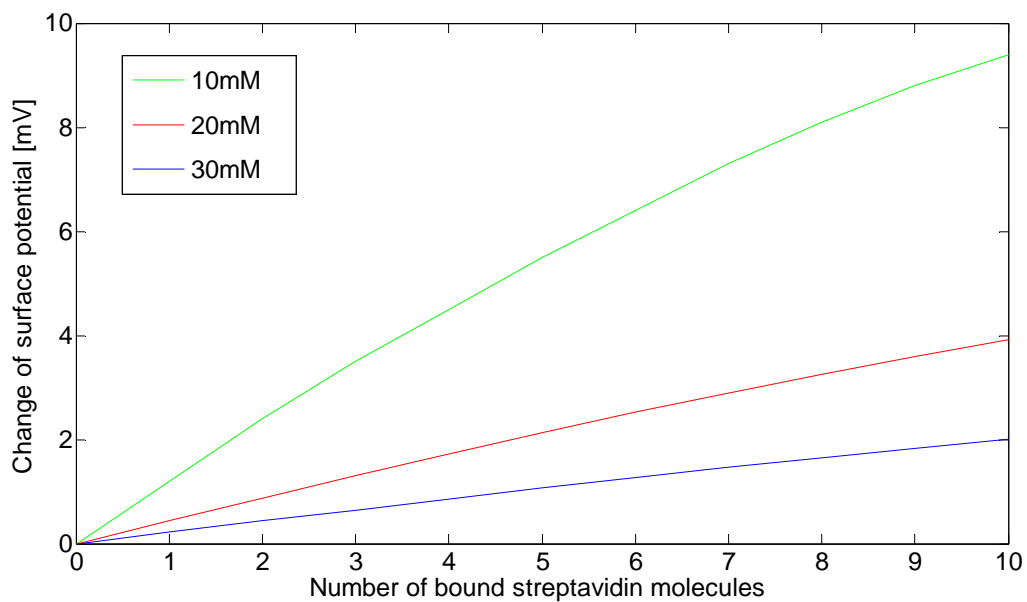
Figure 4.1 Change of silicon oxide surface potential VS. number of streptavidin molecules bound. The inset stands for NaCl concentration.

Table 1. Debye screening lengths VS. different NaCl concentrations

NaCl concentration	Debye screening length (nm)
0.1mM	30.79
1mM	9.74
10mM	3.08
100mM	0.97
1M	0.31
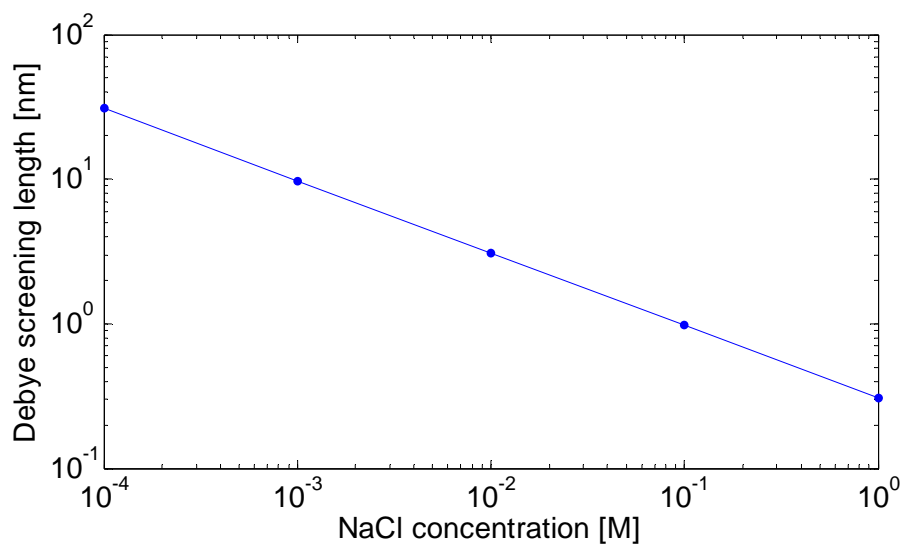
**Figure 4.2** Debye screening lengths VS. different NaCl concentrations
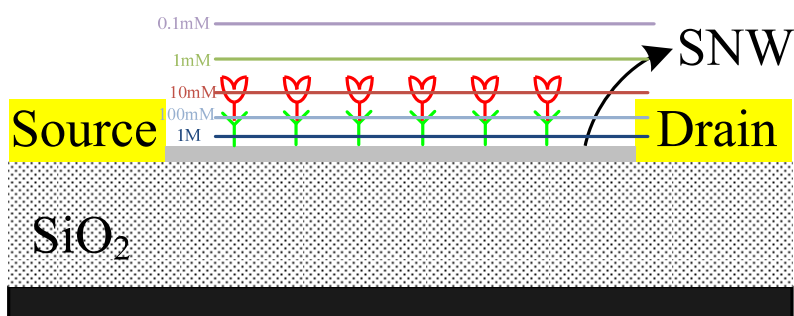
Figure 4.3 Scheme of Debye screening (the distance is not to scale)

The scheme of Debye screening is shown in Figure 4.3. The color lines show the different Debye screening length (from SiNW to the lines) according to different NaCl concentrations. The SiNW can only sense charged molecules within the Debye screening length. The charged molecules beyond the Debye screening length will be screened by the ions in the electrolyte. As can be seen, NaCl concentrations of 1M, 100mM and 10mM are not suitable for detection of the biotin/ streptavidin binding because part of the charge on the biomolecules will be screened. This conclusion is confirmed in Figure 4.1. Without varying other parameters, higher NaCl concentrations result in smaller change of silicon oxide surface potential.

The I-V characteristics of the SiNW FET biosensor are calculated by solving the Poisson equation and then drift-diffusion equation using a MuGFET simulator [67]. MuGFET is a simulation tool for nano-scale multi-gate FET structure and SiNW FET. It provides self-consistent solutions to the Poisson and drift-diffusion equation via a user-friendly graphical user interface.

We assume the source and drain extension of the SiNW is 10nm, and the source and drain are n-type doped with doping concentration $10^{18}cm^{-3}$. The source electrode is grounded. In our simulation for the silicon oxide surface voltage change, the reference voltage on the silicon oxide surface (the initial gate voltage for the SiNW FET) is around 0.4V. Binding of the streptavidin molecules leads the gate voltage change of several mV. It is important to find a proper drain voltage to make the SiNW FET to work in a point which is very sensitive to the gate voltage change, i.e., small change in the gate voltage will lead to big change in the drain current so that the drain current change is appreciable.

We calculate the I-V characteristics for three different gate voltages (Vg=0.40V, 0.41V, 0.42V) while keeping the following parameters constant: SiNW diameter d=10nm, channel doping density $p=10^{15}cm^{-3}$.
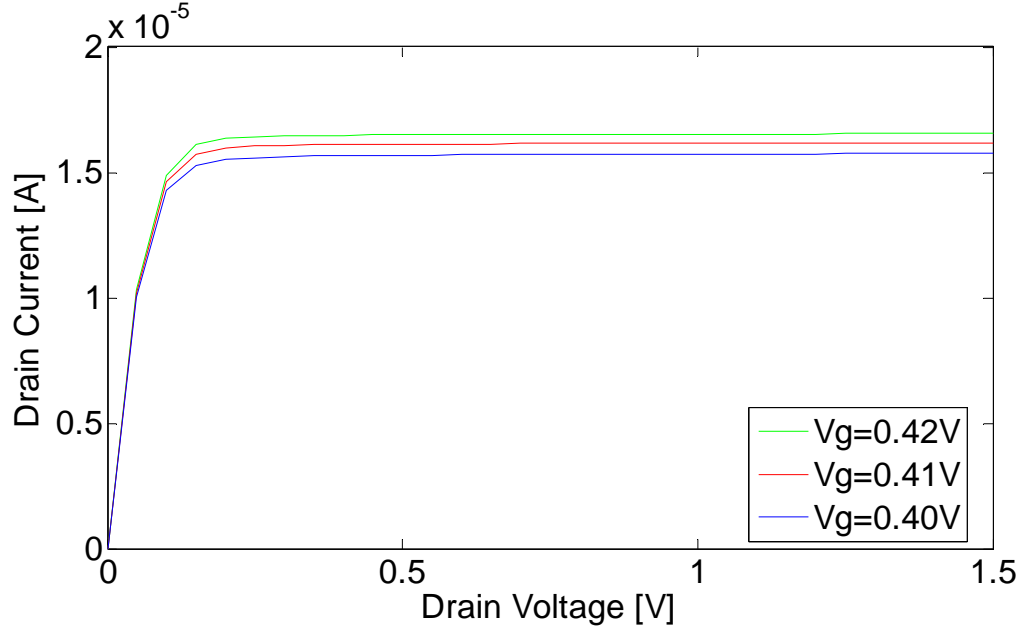
Figure 4.4 The I-V characteristics for different gate voltages

The calculated I-V characteristic is shown in Figure 4.4. As can be seen, when the drain voltage is small, the SiNW FET works in the linear region and the drain current change for different gate voltage is very small. When the drain voltage is big enough, the SiNW FET works in the saturation region and the drain current change for different gate voltage is distinct. Thus, the SiNW FET should work in the saturation region to get a good sensitivity for the gate voltage change. In the rest simulations, we will fix the drain voltage as 1 V to make sure the SiNW FET work in saturation region.

We define the drain current change for different silicon oxide surface potentials (gate voltages) as:

$$\Delta I_d = \frac{I_d(n) - I_d^{ref}}{I_d^{ref}} \times 100\% \quad (4.2)$$

where n denotes the number of streptavidin molecules bound to the avidin molecules, I_d^{ref} is the reference drain current when no streptavidin molecules are bound to the avidin molecules. The drain current change can be regarded as the sensitivity of the SiNW FET biosensor.
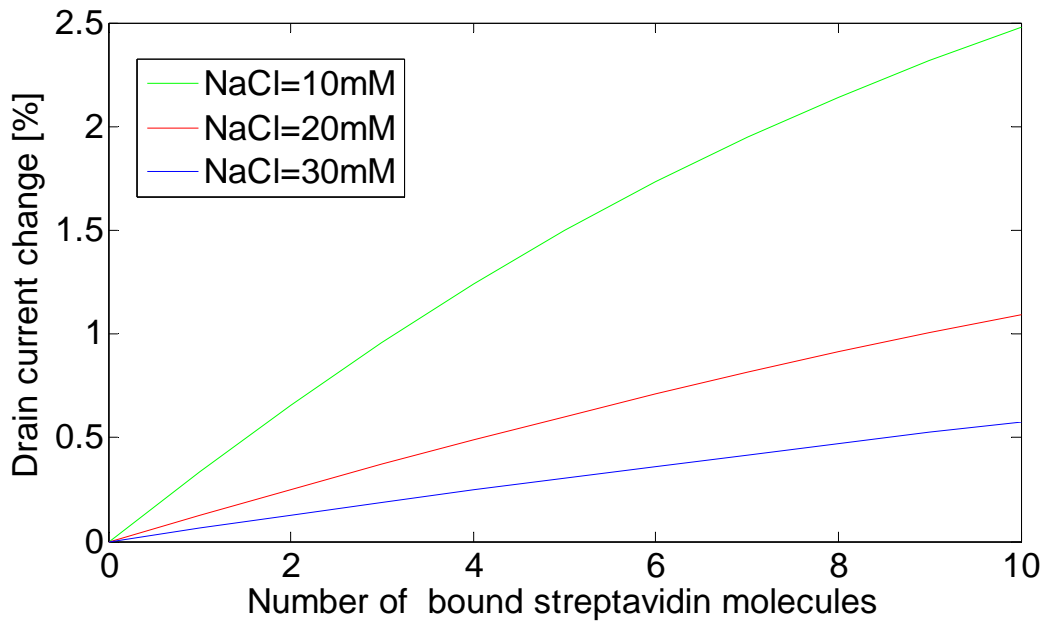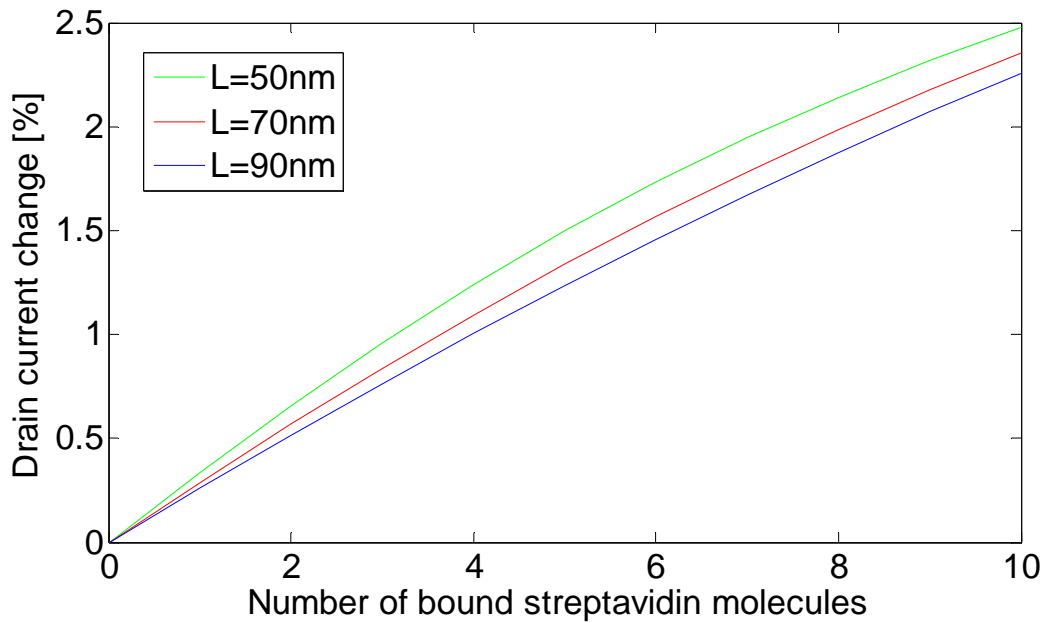
Figure 4.5 Drain current change VS. number of streptavidin molecules bound for different NaCl concentration

Figure 4.5 shows the drain current change according to the number of bound streptavidin molecules for different NaCl concentration. As can be seen, lower concentration of NaCl will lead to large change of silicon oxide surface potential and consequently larger drain current change. Thus, we can reach the conclusion that lower NaCl concentration will result in higher sensitivity of the SiNW FET biosensor.

Using the similar procedure, we investigate the influence of SiNW length to the sensitivity of the SiNW FET biosensor while keeping the following parameters constant: SiNW diameter d=10nm, doping density $p=10^{15}cm^{-3}$ and the NaCl concentration in the electrolyte is 10mM. Three different SiNW lengths (L=50nm, 70nm and 90nm) are investigated and the results are shown in Figure 4.6.

As can be seen, SiNW with shorter length has higher sensitivity. This is reasonable since for shorter SiNW, the traveling speed of carriers is faster and there will be less carriers recombination.

Figure 4.6 Drain current change VS. number of streptavidin molecules bound for different SiNW lengths
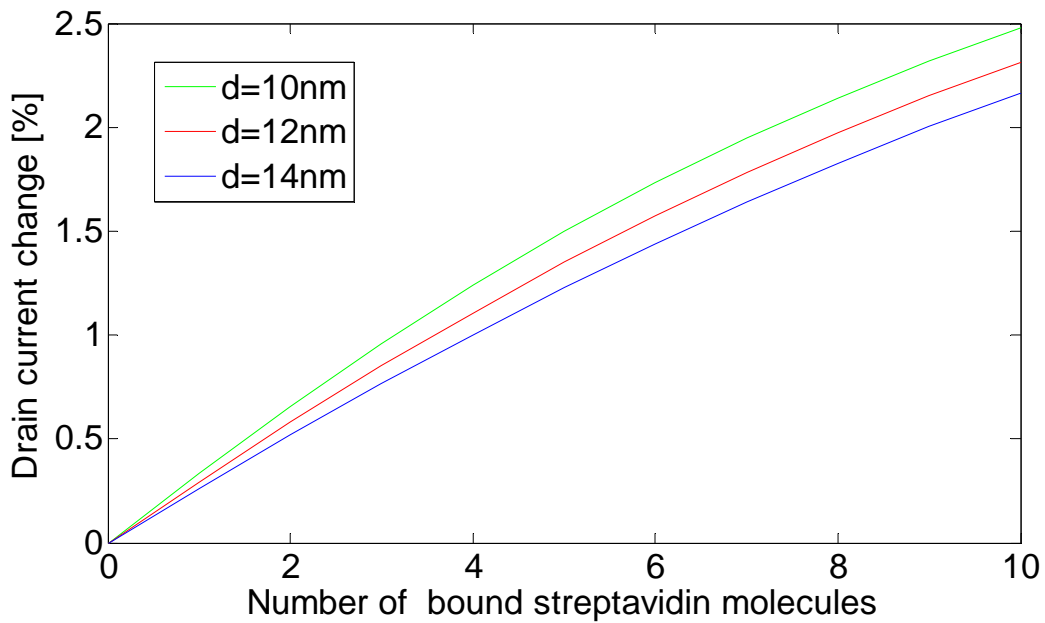
Figure 4.7 Drain current change VS. number of streptavidin molecules bound for different SiNW diameters

The influence of SiNW diameter to the sensitivity of the SiNW FET biosensor is investigated while keeping the following parameters constant: SiNW length L=50nm, doping density $p=10^{15}cm^{-3}$ and the NaCl concentration in the electrolyte is 10mM. Three different SiNW

diameters (d=10nm, 12nm and 14nm) are investigated and the results are shown in Figure 4.7. As can be seen, SiNW with smaller diameter shows higher sensitivity. This is justifiable since for thinner SiNW, the gate voltage has better control over the conducting channel inside the SiNW.
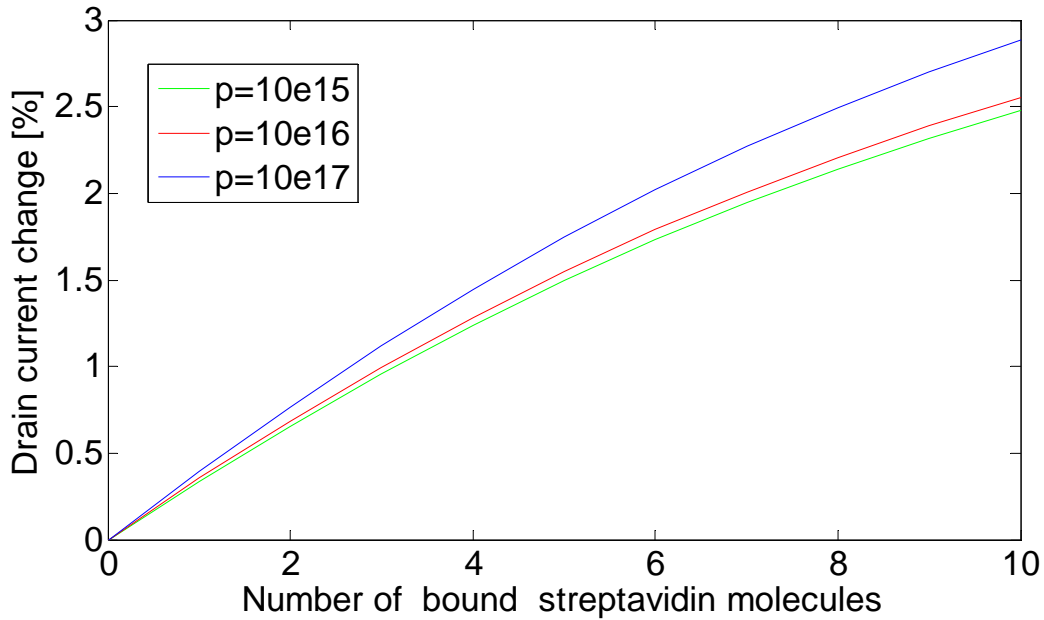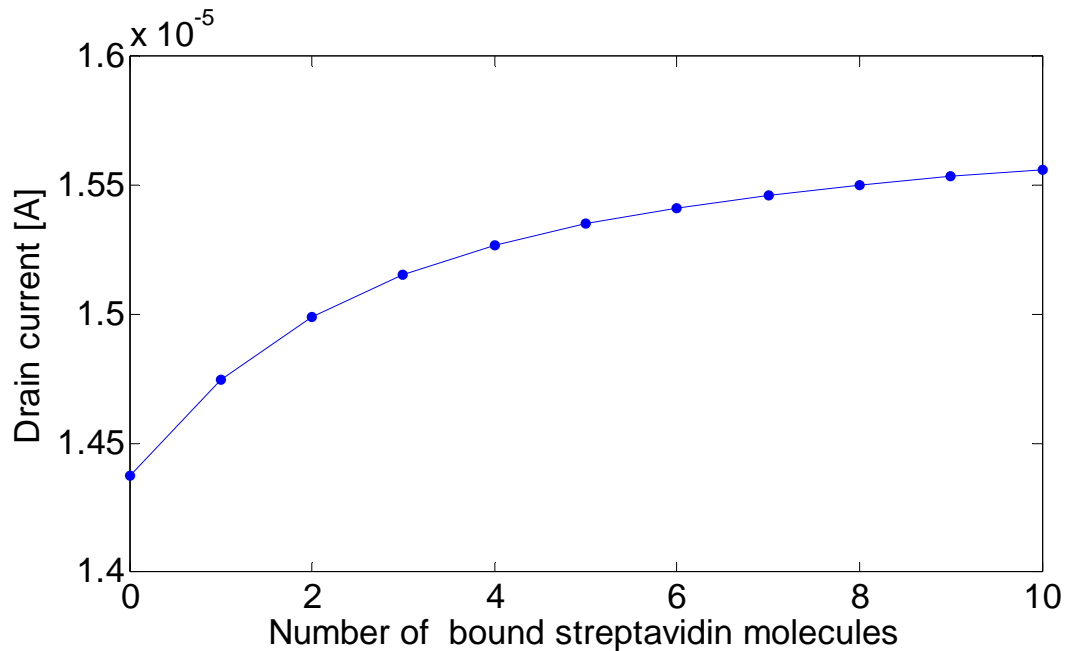

Figure 4.8 Drain current change VS. number of streptavidin molecules bound for different doping levels

The influence of doping levels to the sensitivity of the SiNW FET biosensor is investigated while keeping the following parameters constant: SiNW diameter d=10nm, length L=50nm and the NaCl concentration in the electrolyte is 10mM. Three different doping levels (p=10^{15}cm^{-3}, 10^{16}cm^{-3} and 10^{17}cm^{-3}) are investigated and the results are shown in Figure 4.8. As can be seen, SiNW with higher doping level shows higher sensitivity. This is consistent with equation (4) in [1] where the sensitivity is inversely proportional to the donor concentration and thus is directly proportional to the acceptor (p-type doping) concentration.

Figure 4.9 Drain current VS. number of streptavidin molecules bound

From the above discussion, we can conclude that SiNW with shorter length, smaller diameter, higher doping level and works in electrolyte with lower NaCl concentration has higher sensitivity. When these parameters are properly chosen, it is possible to achieve single streptavidin molecule detection. The following parameters are chosen for a SiNW FET biosensor: SiNW diameter d=10nm, length L=50nm, doping level $p=10^{15}cm^{-3}$ and the NaCl concentration in the electrolyte is 1mM. With nowaday technology, SiNW FET biosensor with these parameters can be readily fabricated. The drain current according to the number of streptavidin molecules bound is shown in Figure 4.9. When the number of the bound streptavidin molecules changes from 0 to 1, the drain current changes by 2.59%, since this change is in measurable range, thus recognition of single streptavidin molecule is feasible. Actually, the sensitivity can be even higher when higher doping level is chosen.

5.0   CONCLUSION AND FUTURE WORK

5.1   CONCLUSION

SiNW FET biosensors can provide direct, label free, high sensitive, high selective, real time and high throughput analysis of biological processes and are gaining importance due to their large potential in commercial applications, ranging from detection of protein, virus and DNA to the discovery of new drug delivery systems.

Lack of fundamental theory to account for the underlying mechanism of electrical sensing of biomolecules hinders the design, optimization and development of the SiNW FET Biosensor.

In this work, using the biotin/streptavidin system as a model system, a comprehensive modeling theory and simulation approach is presented to account for the underlying detection mechanism of biotin/Streptavidin binding using SiNW FET biosensor.

The theory is based on drift-diffusion equation of the SiNW and Poisson Boltzmann equation for the biomolecules and solvent system. The Poisson Boltzmann equation is derived from the classical Poisson equation using the Boltzmann distribution to model the charge distribution in the ionic solvent. The analytical and numerical solutions to the Poisson Boltzmann equation are discussed.

The detailed structures, modeling procedure and simulation methods of the SiNW FET biosensor are presented. The simulation results are analyzed and the influence of parameters like the dimension of the SiNW (diameter and length), the doping level of the SiNW, and surrounding environment (the ions concentration in the solvent) are investigated for the performance optimization of the SiNW FET biosensor. Also, the detection limit of biotin/Streptavidin binding using the SiNW FET biosensor, i.e., the detection of single streptavidin molecule binding is investigated. The preliminary simulation results indicate that the optimal sensor performance can be ensured by careful optimization of its parameters and it is feasible to detect binding of single streptavidin molecule when optimal parameters are chosen. And there is a large room for the sensitivity to be further improved.

The modeling procedure and simulation methods shown in this work can be readily modified and adopted for detection of other receptor-target biomolecules pairs, such as ssDNA-dsDNA antibody-protein and antibody-virus, using SiNW FET biosensor.

The simulation results can serve as a guideline for the design and optimization of SiNW FET biosensor in our future work. The parameters of SiNW chosen for single streptavidin detection can be readily achieved in the NanoScale Fabrication and Characterization Facility (NFCF) at the University of Pittsburgh. Thus, high performance SiNW FET biosensor can be easily fabricated. Since the SiNW FET can be arrayed and modified with different kinds of receptor molecules, it is promising to integrate the SiNW FETs into electrically addressable sensor arrays for multiplexed detection.

5.2   FUTURE WORK

This work shows a preliminary method to model and simulate the SiNW FET biosensor. Several problems need to be addressed in our future work.

First, the Gouy-Chapman theory is suitable for solving the NPBE for a one dimension planar ISFET biosensor and it has shown very good accuracy for this particular case. However, it is an approximation to solve the NPBE for a SiNW FET biosensor using Gouy-Chapman theory, and the accuracy cannot be guaranteed. The biotin and streptavidin molecules are modeled as spheres in this study, differing from their original structures. The charge distribution based on the sphere model is not accurate. In our future work, the biotin and streptavidin molecules will be modeled using their exact structures and a 3D Poisson-Boltzmann equation solver will be used to solve the NPBE for the SiNW-Biomolecules-electrolyte system. This can lead to more accurate result of electrostatic potential change on the silicon oxide surface and hence more accurate calculation of the sensitivity of the SiNW FET biosensor.

Second, the electrolyte is simplified as NaCl solution in this work. This simplification easies the modeling and simulation process but results in inaccurate estimation of the electrostatic potential. The electrolyte actually used in biological experiments is Phosphate Buffered Saline (PBS buffer) which contains NaCl, KCl, Na_2HPO_4, KH_2PO_4. The pH of PBS buffer is 7.4 instead of 7. Also, calculation of Debye screening length will be more complicated for the PBS buffer. In the future, PBS buffer will be used to replace NaCl in the modeling and simulation.

Moreover, in this work, we only consider the static binding of biotin/ streptavidin molecules. And we assume all the streptavidin molecules bind to the center of SiNW. However, this is not true in the real case. The streptavidin molecules diffuse in the electrolyte and bind to the biotin receptors at random location and with random binding angle. This binding is a stochastic process

and can be simulated using a Monte Carlo algorithm. Because of the extremely high binding affinity of biotin/ streptavidin system, we ignore the dissociation of biotin/ streptavidin. In the future, the dynamics should be studied and the dissociation of biotin/ streptavidin should be taken into account. Thus, a general model can be constructed for study of other receptor-target molecules systems with lower binding affinity.

Furthermore, the modeling and simulation of the SiNW FET biosensor are very complicated since two systems are coupled together, namely a biological system (the receptor biomolecules, target biomolecules and the ions in the electrolyte) and an electronic system (the SiNW core and the silicon oxide surface). The potential change on the silicon oxide surface will change the carriers' distribution inside the SiNW core. Contrarily, the carriers' redistribution will change the potential on the silicon oxide surface and also the charge distribution in the electrolyte. This is a self-consistent process and the electrostatics of the biosensors should be calculated self-consistently. In our simulation, we use separate procedure to calculate the electrostatic potential on silicon oxide surface and the current inside the SiNW core. This process may result in huge error. In the future work, the biological system and the electronic system should be treated as an entity and the electrostatic potential should be calculated self-consistently.

Lastly, after all the work mentioned above is done, samples SiNW FET biosensor need to be fabricated and tested to verify the simulation results. Integrating the SiNW FETs with different kinds of receptor molecules into an addressable sensor arrays for multiplexed detection will be the ultimate object.

APPENDIX

LIST OF RESULTING PUBLICATION

1. Yucai Wang and Guangyong Li, "Simulation of a Silicon Nanowire FET Biosensor for Detecting Biotin/Streptavidin Binding", accepted by IEEE NANO 2010, Seoul, Korea, August 2010

2. Yucai Wang and Guangyong Li, "Performance Investigation for a Silicon Nanowire FET Biosensor Using Numerical Simulation", submitted to IEEE Nanotechnology Materials and Devices Conference, Monterey, USA, December 2010

BIBLIOGRAPHY

[1]. Pradeep R. Nair, and Muhammad A. Alam, "Design considerations of silicon nanowire biosensors", IEEE TRANSACTIONS ON ELECTRON DEVICES, 54 (12), Dec. 2007

[2]. P. Bergveld , Development, "operation and application of the ion sensitive field effect transistor as a tool for electrophysiology", IEEE Trans. Biomed. Eng. BME-19 (1972), pp. 342–351

[3]. Clemens Heitzinger, and Gerhard Klimeck, "Computational aspects of the three-dimensional feature-scale simulation of silicon-nanowire field-effect sensors for DNA detection", Journal of Computational Electronics , (2007), 6:387-390

[4]. S. J. Han, H. Yu, R. J.Wilson, R. L. White, N. Pourmand, and S. X.Wang, "CMOS integrated DNAMicroarray based on GMR sensors," IEDM Tech. Dig., 2006, pp. 719–723.

[5]. P. Bergveld, "Thirty years of ISFETOLOGY—What happened in the past 30 years and what may happen in the next 30 years," Sens. Actuators B, Chem., vol. 88, no. 1, pp. 1–20, Jan. 2003.

[6]. Yi Cui, Qingqiao Wei, Hongkun Park, Charles M. Lieber, "Nanowire Nanosensors for Highly Sensitive and Selective Detection of Biological and Chemical Species", SCIENCE VOL 293 17 AUGUST 2001

[7]. Norman A. Lapin and Yves J. Chabal, "Infrared Characterization of Biotinylated Silicon Oxide Surfaces, Surface Stability, and Specific Attachment of Streptavidin", J. Phys. Chem. B, 2009, 113 (25), pp 8776–8783

[8]. Fogolari F, Brigo A, Molinari H., "The Poisson–Boltzmann equation for biomolecular electrostatics: a tool for structural biology", J Mol Recognit 15(6):377–392, 2002

[9]. P. Bergveld , "ISFET, Theory and Practice", IEEE SENSOR CONFERENCE TORONTO, OCTOBER 2003

[10]. G. Moore, "Cramming More Components onto Integrated Circuits," Electronics, vol. 38, no.8, pp. 114-117, 1965.

[11]. International Technology Roadmap for Semiconductors: Executive Summary 2007 Edition. Semiconductor Industry Association: http://public.itrs.net; 2007.

[12]. S. E. Thompson et al., "A logic nanotechnology featuring strained silicon," IEEE Electron Device Lett., vol. 25, pp. 191–193, 2004.

[13]. Y. Kim, et al., "Conventional n-channel MOSFET devices using single layer HfO2 ZrO2 as high-k gate dielectrics with polysilicon gate electrode," in IEDM Tech. Dig., pp.455-458, 2001.

[14]. B. Cheng, M. Cao, R. Rao, et al., "The impact of high-k gate dielectrics and metal gate electrodes on sub-100 nm MOSFETs," IEEE Trans. Electron Devices, vol. 46, pp.1537-1544, July 1999.

[15]. B. Doris, M. Ieong, T. Kanarsky, et al., "Extreme scaling with ultra-thin Si channel MOSFETs," in *Int. Electron Devices Meeting Tech. Dig.*, pp. 267–270.

[16]. Y.-K. Choi, N. Lindert, P. Xuan, et al., "Sub-20 nm CMOS FinFET technologies," in Int. Electron Devices Meeting Tech. Dig., pp. 421–424, 2001.

[17]. B.S. Doyle, S. Datta, M. Doczy, et al., "High performance fully-depleted tri-gate CMOS transistors," IEEE Electron Device Lett., vol. 24, no. 4, pp. 263-265, Apr. 2003.

[18]. Chau, R., Datta, S., Doczy, M., et al., "Benchmarking Nanotechnology for High Performance and Low-Power Logic Transistor Applications", IEEE Trans Nanotechnology 2005, 4, 153–158.

[19]. Chau, R., Doyle, B., Datta, S., et al., "Integrated Nanoelectronics for the Future", Nat. Mat. 2007, 6, 810–812.

[20]. Goldberger, J.; Hochbaum, A. I.; Fan, R.; Yang, P. D. Silicon Vertically Integrated Nanowire Field Effect Transistors. Nano Lett. 2006, 6, 973–977.

[21]. Baxendale, M. Carbon Nanotubes and Bucky Materials. In Springer Handbook of Electronic and Photonic Materials. Springer: New York, 2006, 1147–1154.

[22]. Boukai, A. I., Bunimovich, Y., Tahir-Kheli, J.,et al., "Silicon Nanowires as Efficient Thermoelectric Materials", Nature 2008, 451, 168–171.

[23]. Lieber, C. M. "Nanoscale Science and Technology: Building a Big Future from Small Things", MRS Bull. 2003, 28, 486–491.

[24]. Yu, J. Y., Chung, S. W., Heath, J. R., "Silicon Nanowires: Preparation, Device Fabrication, and Transport Properties", J. Phys. Chem. B 2000, 104, 11864–11870.

[25]. Melosh, N. A., Boukai, A., Diana, F., et al., "Ultrahigh-Density Nanowire Lattices and Circuits", Science 2003, 112–115.

[26]. Gudiksen, M. S., Lauhon, L. J., Wang, J., et al., "Growth of Nanowire Superlattice

Structures for Nanoscale Photonics and Electronics. Nature 2002, 415, 617–620.

[27]. McAlpine, M. C., Friedman, R. S., Jin, S.,et al., "High-Performance Nanowire Electronics and Photonics on Glass and Plastic Substrates", Nano Lett. 2003, 3, 1531–1535.

[28]. Y. Cui, Z. Zhong, D. Wang, W. Wang, and M. Lieber, "High performance silicon nanowire field effect transistors," Nano Lett., vol. 3, pp. 149-152, 2003

[29]. S. W. Chung, J. Y. Yu, J. R. Heath, "Silicon nanowire devices," Appl. Phys. Lett. vol. 76, pp 2068-2070, 2000.

[30]. N. Singh, "Gate-all-around MOSFETs: lateral ultra-narrow ($\leqslant$ 10 nm) fin as channel body,"
Electronics Letters, v. 41 issue 24, pp. 1353, 2005.

[31]. N. Singh. "High-performance fully depleted silicon nanowire (diameter $\leqslant$ 5 nm) gateall-around CMOS devices." IEEE Electron Device Letters, v. 27 issue 5, pp. 383, 2006.

[32]. V. Schmidt, H. Riel, S. Senz, S. Karg, W. Riess and U. Gosele, "Realization of a silicon nanowire vertical surround-gate field-effect transistor," Small, vol. 2, pp. 85, 2006.

[33]. https://nanohub.org/tools/nanofinfet

[34]. Fernando Patolsky, Gengfeng Zheng and Charles M Lieber, "Fabrication of silicon nanowire devices for ultrasensitive, label-free, real-time detection of biological and chemical species", NATURE PROTOCOLS, VOL.1NO.4 2006 1711

[35]. Ward, A.M., Catto, J.W.F. and Hamdy, F.C. "Prostate specific antigen: biology, biochemistry and available commercial assays", Ann. Clin. Biochem. 38, 633–651(2001).

[36]. Mirkin, C.A. et al., "A DNA-based method for rationally assembling nanoparticles into macroscopic materials", Nature 382, 607–609 (1996).

[37]. M. E. Davis and J. A. McCammon, "Electrostatics in biomolecular structure and dynamics", Chem. Rev., 90 (1990), pp. 509-521.

[38]. Fogolari F, Brigo A, Molinari H, "The Poisson-Boltzmann equation for biomolecular electrostatics: a tool for structural biology", J Mol Recognit. 2002 Nov-Dec;15(6):377-92.

[39]. P. Debye and E. H uckel, Physik. Z., 24 (1923), p. 185.

[40]. W. B. CHESTON, Elementary theory of electric and magnetic fields, John Wiley& Sons, Inc., 1964, ch. 2–5.

[41]. Paris, R. B. & Kaminsky, D. (2001), Asymptotics and the Mellin-Barnes Integrals, New York: Cambridge University Press

[42]. Rahul S Sampath, A Study of the Poisson-Boltzmann Equation and its Applications in the Sensitivity Analysis of VCP/SPICE, http://www.cc.gatech.edu/~rahulss/index_files/indRepFinal.pdf

[43]. Peter Atkins and John W. Locke, Atkins' Physical Chemistry, Oxford University Press; 7th edition (January 2002)

[44]. http://en.wikipedia.org/wiki/Maxwell%E2%80%93Boltzmann_statistics

[45]. K. Forsten et al., "Numerical Solution of the Nonlinear Poisson-Boltzmann Equation for a Membrane-Electrolyte System", J. Phys. Chem.1994, 98, 5580-5586

[46]. A. SAYYED-AHMAD, K. TUNCAY, AND P. J. ORTOLEVA, "Efficient solution technique for solving the poisson-boltzmann equation", J. Comput. Chem., 25 (2004), pp. 1068–1074.

[47]. S. S. KUO, M. D. ALTMAN, AND J. P. BARDHAN, "Fast methods for simulation of biomolecule electrostatics", IEEE, 0-7803-7607-2/02 (2002), pp. 466–473.

[48]. N. A. BAKER, D. SEPT, M. J. HOLST, AND J. A. MCCAMMON, The adaptive multilevel finite element solution of the poisson-boltzmann equation on massively parallel computers, IBM J. Res. & Dev., 45 (2001), pp. 427–438.

[49]. I. Klapper, R. Hagstrom, R. Fine, K. Sharp and B. Honig, "Focusing of electric fields in the active site of Cu-Zn superoxide dismutase: effects of ionic strength and amino-acid modification", Proteins, 1 (1986)(1), 47–59

[50]. A. Nicholls, R. Bharadwaj and B. Honig. "Grasp-graphical representation and analysis of surface-properties", Biophys. J., 64 (1993) (2), A166–A166

[51]. D. Bashford, "An object-oriented programming suite for electrostatic effects in biological molecules", Lecture Notes in Computer Science, VOL 1343, Springer (1997). pp. 233–240

[52]. J. D. Madura, J. M. Briggs, R. C. Wade, et al., "Electrostatics and diffusion of molecules in solution - simulations with the university-of-houston brownian dynamics program", Comput. Phys. Commun., 91 (1995) (1-3), 57–95

[53]. W. Im, D. Beglov and B. Roux, "Continuum solvation model: Computation of electrostatic forces from numerical solutions to the Poisson-Boltzmann equation", Comput. Phys. Commun., 111 (1998), 59–75

[54]. B. R. Brooks, R. E. Bruccoleri, B. D. Olafson, et al., "Charmm: A program for macromolecular energy, minimization, and dynamics calculations", J. Comput. Chem., 4 (1983), 187–217

[55]. B. Z. Lu1, Y. C. Zhou, M. J.Holst, and J.A.McCammon, "Recent Progress in Numerical

Methods for the Poisson-Boltzmann Equation in Biophysical Applications", Commun. Comput. Phys. Vol. 3, No. 5, pp. 973-1009. May 2008

[56]. S. M. Sze, Physics of Semiconductor Devices. New York: Wiley, 1981

[57]. D. McQuarrie, Statistical Mechanics. New York: Harper & Row, 1976.

[58]. http://www.nextnano.de

[59]. S. Birner et al., "Theoretical model for detection of charged proteins with a silicon-on-insulator sensor", J. Phys.: Conf. Ser. 107 012002, 2008

[60]. D. Winzor, "Protein Charge Determination", Curr Protoc Protein Sci. 2005 Sep;Chapter 2:Unit 2.10.

[61]. H. Jakubke and H. Jeschkeit, AminoAcids, Peptides and Proteins. John Wiley& Sons, New York, 1977

[62]. R. Barbucci et al., "Antigen-Antibody Recognition by Fourier Transform IR Spectroscopy/ Attenuated Total Reflection Studies: Biotin-Avidin Complex as an Example", Biopolymers, Vol.31, 827-834 (1991)

[63]. J. Schiewe et al., "Application and optimization of capillary zone electrophoresis in vitamin analysis", Journal of Chromatography A,1995, Vol. 717, Issues 1-2, Pages 255-259

[64]. B. Skoog and A. Wichman, "Calculation of the isoelectric points of polypeptides from the amino acid composition", trends in analytical chemistry, vol. 5, no. 4, 1986

[65].   http://biophysics.cs.vt.edu/H++

[66]   J. Gordon et al., "H++: a server for estimating pKas and adding missing hydrogens to macromolecules", Nucleic Acids Res. 33, W368-71 (2005)

[67]. S. Kim, G. Klimeck, S.Damodaran, and B. Haley, (2008), "MuGFET," DOI: 10254/nanohub-r3843.3.